ADVANCED INDOOR THERMAL ENVIRONMENT CONTROL USING OCCUPANT'S MEAN FACIAL SKIN TEMPERATURE AND CLOTHING LEVEL

by

Xuan Li

A Thesis

Submitted to the Faculty of Purdue University

In Partial Fulfillment of the Requirements for the degree of

Master of Science in Mechanical Engineering

School of Mechanical Engineering

West Lafayette, Indiana

May 2020

THE PURDUE UNIVERSITY GRADUATE SCHOOL
STATEMENT OF COMMITTEE APPROVAL

Dr. Qingyan Chen, Chair

School of Mechanical Engineering

Dr. Ming Qu

School of Civil Engineering

Dr. Mireille Boutin

School of Electrical and Computer Engineering

Approved by:

Dr. Nicole L. Key

To my parents and my loved one

In memory of those old days

El Psy Congroo

TABLE OF CONTENTS

LIST OF TABLES 6
LIST OF FIGURES 7
ABSTRACT 9
CHAPTER 1. INTRODUCTION 11
1.1 Background and Significance 11
1.2 Literature Review 13
1.2.1 Numerical Models for Clothing Level Measurement 13
1.2.2 Image Classification 14
1.2.3 Evaluation of Thermal Comfort in Indoor Environment 15
1.2.3.1 Rational Models 15
1.2.3.2 Adaptive Models 16
1.2.3.3 Psychological Models 17
1.2.3.4 Physiological Models 19
1.2.4 Physiological Indicators of Thermal Comfort and Measuring Instrument 20
1.3 Outline of this Thesis 23
CHAPTER 2. CLOTHING LEVEL CLASSIFICATION AND COMFORTABLE AIR TEMPERATURE 25
2.1 Clothing Level Classification 25
2.1.1 Pre-trained CNN Model 25
2.1.2 Preparation of the Training Dataset 27
2.1.3 Training of the Image Classification Model 29
2.1.4 Results 31
2.1.5 Discussions 36
2.2 Comfortable Air Temperature 37
2.2.1 Data Collection 37
2.2.2 Results 40
2.2.3 Discussions 44
2.3 Conclusions 45
CHAPTER 3. MEAN FACIAL SKIN TEMPERATURE AND THERMAL COMFORT 46

3.1 Face Detection 46
3.2 Temperature Measurement using Thermographic Camera 48
3.3 Data Collection 52
3.4 Results 53
3.4.1 Face Detection and Temperature Measurement 53
3.4.2 Mean Facial Skin Temperature and Thermal Comfort 57
3.5 Discussions 61
3.6 Conclusions 62
CHAPTER 4. IMPLEMENTATION AND VALIDATION OF THE CONTROL STRATEGY 64
4.1 Implementation of the Control Strategy 64
4.2 Validation of the Control Strategy 71
4.3 Results 72
4.4 Discussions 81
4.5 Conclusions 82
CHAPTER 5. CONCLUSIONS AND FUTURE WORKS 83
5.1 Conclusions 83
5.2 Future Works 84
LIST OF REFERENCES 86
LIST OF PUBLICATIONS 92

LIST OF TABLES

Table 2.1 Structure of MobileNetV2 26
Table 2.2 Clothing insulation value 28
Table 2.3 Hyperparameters for mini-batch gradient descent 31
Table 2.4 Structure of the classifier in Python 33
Table 2.5 Performance of the trained model 36
Table 2.6 Comfortable air temperature for different clothing level 41
Table 2.7 PMV validation results 44
Table 3.1 Specifications of Lepton 3.5 (FLIR, 2020) 51
Table 4.1 Fundamental logic for temperature setpoint adjustment 69
Table 4.2 Number of tests for different types of the results. 73

LIST OF FIGURES

Figure 1.1 Comparison between physiological models (Katić et al., 2016) 19
Figure 2.1 Structure of inverted residual block 26
Figure 2.2 Sample images from retrain dataset: (a) 0.6 *clo* (b) 0.4 *clo* (c) 0.8 *clo* 27
Figure 2.3 Illustration for transfer learning 29
Figure 2.4 Structure of clothing level classifier 30
Figure 2.5 Training dataset (a) Folders for different clothing level (b) Sample images for 0.4 *clo* 32
Figure 2.6 Separation of the dataset 32
Figure 2.7 Results of training 34
Figure 2.8 Average validation accuracy for each epoch 35
Figure 2.9 Sample classification result (a) Input image (b) Classification result 36
Figure 2.10 Location of the office, indicated by the red dot 38
Figure 2.11 Office layout 38
Figure 2.12 Data collection devices (a) Thermostat (b) Data logger. (c) RGB camera 39
Figure 2.13 Raw data of comfortable air temperature 40
Figure 2.14 Second-order parabolic trend line for averaged comfortable air temperature 42
Figure 2.15 PMV calculation tool 43
Figure 3.1 Different shapes of filters for calculating Haar-like feature 46
Figure 3.2 Calculating the sum of the shaded rectangle area 47
Figure 3.3 Haar-cascade face detection structure 48
Figure 3.4 LWIR camera system (a) Thermal camera core (b) I/O module with camera mounted (GetLab, 2020) 50
Figure 3.5 User interface of camera control panel (FLIR, 2020) 52
Figure 3.6 Raw image of the LWIR camera 54
Figure 3.7 MATLAB script for 8-bit conversion 55
Figure 3.8 Image in 8-bit gray scale 55
Figure 3.9 Face detection result 56
Figure 3.10 Temperature conversion results (a) Raw readings (b) Readings in Celsius 56

Figure 3.11 Temperature calculation result (a) Detected face area (b) Calculated temperature .. 57
Figure 3.12 Mean facial skin temperature at different TSV 58
Figure 3.13 Average mean facial skin temperature at different TSV 60
Figure 3.14 Mean temperature on forehead (Choi and Loftness, 2012) 61
Figure 4.1 Front panel of the control system 64
Figure 4.2 Block diagram of control VI 67
Figure 4.3 Control script for acclimation period 68
Figure 4.4 Flowchart of improved control logic 70
Figure 4.5 Implementation of improved control logic 71
Figure 4.6 Type 1 sample results 73
Figure 4.7 Type 2 sample results 76
Figure 4.8 Type 3 sample results 79

ABSTRACT

People spend most of their time indoors. Because people's health and productivity are highly dependent on the quality of the indoor thermal environment, it is important to provide occupants with healthy, comfortable and productive indoor thermal environment. However, inappropriate thermostat temperature setpoint settings not only wasted large amount of energy but also make occupants less comfortable. This study intended to develop a new control strategy for HVAC systems to adjust the thermostat setpoint automatically and accordingly to provide a more comfortable and satisfactory thermal environment.

This study first trained an image classification model based on CNN to classify occupants' amount of clothing insulation (clothing level). Because clothing level was related to human thermal comfort, having this information was helpful when determining the temperature setpoint. By using this method, this study performed experimental study to collect comfortable air temperature for different clothing levels. This study collected 450 data points from college student. By using the data points, this study developed an empirical curve which could be used to calculate comfortable air temperature for specific clothing level. The results obtained by using this curve could provide environments that had small average dissatisfaction and average thermal sensation closed to neutral.

To adjust the setpoint temperature according to occupants' thermal comfort, this study used mean facial skin temperature as an indicator to determine the thermal comfort. Because when human feel hot, their body temperature would rise and vice versa. To determine the correlation, we used a long wave infrared (LWIR) camera to non-invasively obtain occupant's facial thermal map. By processing the thermal map with Haar-cascade face detection program, occupant's mean facial skin temperature was calculated. By using this method, this study performed experimental study to collect occupant's mean facial skin temperature under different thermal environment. This study collected 225 data points from college students. By using the data points, this study discovered different intervals of mean facial skin temperature under different thermal environment.

Lastly, this study used the data collected from previous two investigations and developed a control platform as well as the control logic for a single occupant office to achieve the objective. The

measured clothing level using image classification was used to determine the temperature setpoint. According to the measured mean facial skin temperature, the setpoint could be further adjusted automatically to make occupant more comfortable. This study performed 22 test sessions to validate the new control strategy. The results showed 91% of the tested subjects felt neutral in the office

CHAPTER 1. INTRODUCTION

1.1 Background and Significance

People spend 90% of their time indoors and many spend their time at work in office environments (NHAPS, 2001). In these environments, people's health and productivity was highly dependent on the quality of the indoor thermal environment (Wyon et al., 1987). Therefore, it is very important to provide occupants with healthy, comfortable and productive indoor thermal environments.

Nowadays, such environments are usually provided by using heating, ventilation and air conditioning (HVAC) systems. Such environments are usually provided by using heating, ventilation and air conditioning (HVAC) systems. As a result, the demand of HVAC systems in providing high quality indoor environment leads to a greater energy consumption. Specifically, in the United States, 44% of the energy consumed by commercial buildings was used for heating, cooling and ventilation as the year of 2012 (EIA, 2019). One reason that made HVAC systems consumed so much energy was the control strategy.

Currently, in many buildings, the building automation systems (BAS) controlled the HVAC systems to provide specific air temperature which was usually determined by using setpoint temperature control (Kontes et al., 2017), and the setpoint control was usually combined with a scheduling system to only operate the HVAC during work hours (8 a.m. to 5 p.m.) (Haniff et al. 2013). However, Erickson et al. (2009, 2010) pointed out that fixed time-scheduling strategy would waste energy because it would control the spaces regardless occupancy status. Furthermore, with such amount energy consumed by the HVAC systems, many occupants were still not happy with their indoor thermal environments provided by the HVAC systems. For example, a study indicated only 35% occupants were satisfied with their air temperature supplied in the offices (Putra, 2017). Another survey also concluded that people felt cold or hot more often in offices than homes (Krajalainen, 2009). Thus, it is important to improve the current control strategy to provide more comfortable thermal environments for occupants.

Thermal sensation describes the physiological and subjective response of occupants to the thermal environment in buildings (Arens et al., 2006). To evaluate thermal sensation, one can use the predicted mean vote (PMV) and predicted percentage of dissatisfaction (PPD) model (Fanger,

1982). In this model, it concluded six factors that related to occupants' thermal sensation which were: air temperature, air velocity, relative humidity, mean radiant temperature, metabolic rate and clothing level (thermal insulation provided by clothing with a unit of *clo*). This model suggested that these six parameters should all be considered to provide the most comfortable thermal environment. However, current setpoint temperature control did not consider occupant's clothing level when determining the setpoint. According to Arens et al. (2010), the setpoint temperatures were mainly determined by standards such as ASHRAE Standard 55 and ISO 7730, and in those standards the temperature setpoint were only designed for two clothing levels (ASHRAE, 2013; ISO, 2005). Moreover, studies pointed out the clothing levels were not constantly and uniformly distributed among groups (Nicol and Humphreys 2002). Therefore, current setpoint temperature control could make individual with different clothing level uncomfortable. Hence, it is essential to consider occupant's clothing level when determining the setpoint temperature in the control strategy to make occupant more comfortable.

Another major issue of the current HVAC control strategy was that temperature setpoint could not be automatically adjusted to meet occupants' needs. In most of the commercial offices, the thermostats were usually placed away from the occupants. Such situation discouraged the occupants to tune the temperature setpoint even though they preferred a different temperature and the occupant would feel less comfortable. Also, the temperature measured at that location was not the temperature that occupants sensed. Therefore, Brager et al. (2015) criticized that the current control method did not consider occupants' thermal comfort. Meanwhile, among those who willingly to adjust the setpoints, the setpoints were usually changed to awkward values due to the lack of understanding of the HVAC systems (Peffer, et al., 2011). For example, when occupants felt hot, they might adjust the temperature setpoint to extremely low because they thought the system could cool the room faster, however, after a while, they might think the room was too cold and they needed to adjust temperature setpoint again. Such behavior not only made occupants more uncomfortable but also introduced unnecessary load to the HVAC system which wasted ten billion dollars per year in the US (Derrible and Reeder, 2015). Therefore, it is worthwhile to determine occupants' real-time thermal sensation for the control strategy to adjust the setpoint temperature automatically and accordingly.

1.2 Literature Review

To accurately and quickly obtain the information about occupant's clothing level and thermal comfort is critical for the new control strategy to provide comfortable environment. Therefore, it is worthwhile to develop new methods and models to obtain the information. This goal required good understanding of the state-of-the-art methods and models. Thus, this section explained the literature review on related researches.

1.2.1 Numerical Models for Clothing Level Measurement

Most of the studies used questionnaire (Fanger, 1982; Gagge, 1971; Yao et al., 2009) to collect occupant's clothing level. However, survey method could not obtain occupant's clothing level conveniently and timely, because occupants needed to interrupt their work to report their clothing level. Thus, it is necessary to investigate non-invasive ways to obtain occupant's indoor clothing level information.

Schiavon and Lee (2013) developed two linear models to inversely predict indoor clothing level based on outdoor air and indoor operative temperature, respectively. Two developed models explained 19% and 22% of the variance in clothing insulation, respectively. Carvalho et al. (2013) used linear model to predict indoor clothing level, but they only concluded that clothing level was mostly dependent on the average outdoor temperature of the previous day. Liu et al. (2018) used exponentially weighted running mean (RM) of the past outdoor and a four parameters logistic function to fit the relation between indoor clothing insulation and the RM outdoor temperatures. The model explained 90% of the variance in clothing insulation. Ngarambe et al. (2019) developed a deep neural network to predict indoor clothing level based on outdoor environment factors and mode of transportation. The deep neural network method explained 90% of the variance in clothing insulation.

These studies regarded clothing level as a dependent variable of environmental parameters and developed models to predict clothing level. However, people also consider what occasions they are going to present and what activities they are going to do when choosing clothes. These personal adjustments were not considered in existing models which limited the performance of these models. Furthermore, existing numerical models could only predict average indoor clothing level for specific outdoor climate which means the models couldn't determine real-time clothing level. Thus,

it is necessary to find a new approach rather than using numerical models to measure real-time clothing level to provide a more comfortable environment.

1.2.2 Image Classification

To determine real-time clothing level, numerical models were not a good approach, thus this study took a different approach which was using visual content to determine clothing level. Normally, different clothes have different looks, for example, T-shirts and sweatshirts. People could quickly tell what kind of clothes others were wearing. Thus, distinguish clothes by human eye was possible.

However, it was infeasible to assign a person to determine other's clothing level in real. Thus, an automatic agent was required to perform such tasks. Thanks to the development of computer vision, computers could classify an object in an image based on the visual contents (also known as image classification) using special programs. Thus, this study intended to investigate the approach of using image classification program to determine occupant's clothing level.

Image classification refers to the task of classifying objects in images based on their visual contents. For example, an image classification program could tell the species of a flower in a picture. Nowadays, the most popular way to perform image classification is by using artificial neural networks (ANNs). Among them, the convolutional neural networks (CNNs) had become a major in completing image recognition, classification and detection tasks (Rawat and Wang, 2017). In 1989, LeCun et al. proposed the first CNN with multiple layers to process handwritten digit images. Their CNN was used to classify U.S. zip code. But the accuracy was low. Later in 1998, LeCun et al. developed a new CNN architecture called LeNet-5. It had a good performance using the dataset called Modified National Institute of Standards and Technology (MNIST) which contains 70,000 handwritten digits.

However, CNNs stopped to develop due to limited computational power (Simard et al. 2003). Until recent years, thanks to the advances in computing machines, CNNs with more complicated structures were developed. Ranzato et al. (2007) introduced an architecture to extract hierarchical sparse features using max pooling technique. It achieved an 0.64% error on the MINST dataset. Lin et al. (2013) developed a CNN with convolutional filters replaced by multilayered perceptrons. This network produced state-of-the-art classification performances on Canadian Institute for Advanced Research dataset with 10 classes (CIFAR-10) and CIFAR-100 datasets. Furthermore,

Simonyan and Zisserman (2014) focused on deeper or more complicated network. They used methods including dimension reduction and residual network to improve the classification accuracy. As a result, their network had an enhanced accuracy on ImageNet dataset (the largest dataset in the field of image classification) but had a higher computational cost. These studies proved that modern CNN models achieved high accuracy on image classification.

Based on the research, there was only one study that used CNN to perform clothing classification and it could only classify the style of clothes (i.e. T-shirt, shoes, shorts, etc.). Schindler et al. (2018) used CNN to classify fashion and apparel. They used multiple CNN models and the average accuracy for 30 types of clothes and the best accuracy was 91.07%. However, because this study could only classify the style, it was not helpful to classify clothing level. Thus, it is necessary to build our own image classification model in this study to measure clothing level.

1.2.3 Evaluation of Thermal Comfort in Indoor Environment

Thermal comfort had a definition as follow: the condition of mind which expresses satisfaction with the thermal environment and is assessed by subjective evaluation (American Society of Heating, Refrigerating and Air-Conditioning Engineers (ASHRAE), 2013). Thermal comfort as a subjective sense was extremely hard to evaluate using numerical parameters, however, the comfortable temperature for different people but with similar conditions such as clothing, humidity was found to be similar (ASHRAE, 2013). Therefore, multiple numerical models that related thermal comfort with different environment parameters have been developed in last 50 years. There were four main approaches that researchers followed to develop human thermal comfort models which were rational approach, adaptive approach, psychological approach and physiological approach (Enescu, 2017).

1.2.3.1 Rational Models

The rational approach, also known as heat-balance approach, based on the steady-state experiments which revealed that hot discomfort was caused by skin wittedness and clod discomfort was caused by mean skin temperature (Djongyang et al., 2010). Based on these findings, Fanger (1982) developed the most famous thermal comfort model known as the predicted mean vote (PMV) and percentage of dissatisfaction (PPD) model. The PMV model could predict the mean

value (mean vote) of the feeling responded by all the subjects under given condition. The vote in this model referred to the 7-scale thermal sensation vote (TSV) (−3 for cold, −2 for cool, −1 for slightly cool, 0 for neutral, + 1 for slightly warm, + 2 for warm, and + 3 for hot) determined by the ASHRAE standard (2013). The PPD model could predict the percentage of people who felt uncomfortable at specific PMV. For example, the PPD model predicted that 100% people would be dissatisfied if the PMV was ±3. Another contribution of this model was that it concluded six parameters that related to the thermal comfort or PMV. The six parameters were: air temperature, air velocity, mean radiant temperature, relative humidity, metabolic rate and clothing level. However, because this model was developed from climate chamber with steady-state environment, researchers like McIntyre (1978) raised suspects toward the reliability of the steady-state model developed by Fanger. Because certain variables in the study was not reproduceable in real life. Similarly, Schiavon and Melikov. (2008) also proved it was impossible to create climate-chamber-like environment in real life. Regardless these doubts, the PMV-PPD model was still the most popular model used in thermal comfort study, but researches started to develop adaptive models under environments that were more realistic.

1.2.3.2 Adaptive Models

The adaptive models referred to those models that were not developed in climate chamber but in different environments by field study (Djongyang et al., 2010). De Dear and Brager (2001) first published an adaptive model of thermal comfort which was developed from field study and concluded the dependence of indoor air thermal comfort on outdoor air temperatures especially in natural ventilated buildings. Ogbonna and Harris (2008) performed empirical thermal comfort study in Jos, a city located in tropical sub-Saharan Africa. They collected the data including air temperature, humidity, CO_2 level and lighting level, as well as questionnaires on occupants' sensations of thermal comfort. They concluded that an operative temperature of 26.67 °C would be the best at that specific location. Chu and Jong (2008) developed the least enthalpy estimator (LEE) which combined the concept of human thermal comfort with enthalpy theory to predict thermal comfort. They concluded that the HVAC systems operated under settings generated by the LEE could provide comfortable environment while saving the energy. Pasupathy et al. (2008) investigated technologies which were affordable and efficient that could be used to store large amounts of heat or cold with a small size. In their study, they found that increasing the thermal

storage capacity of a building could increase human comfort by decreasing the frequency of internal air temperature swings and maintained the indoor air temperature at the desired temperature for a longer period. Yao et al. (2009) developed Adaptive PMV (aPMV) for Chongqing, a city in China, to compensate the poor performance of PMV model under hot and humid environment. Their model used only one input which was the mean outdoor temperature to calculate the optimum operative temperature. Similarly, Indraganti et al. (2014) developed an adaptive model for hot and humid climates of India. Their model provided a relationship between comfortable temperature and running mean of the outdoor temperature. Xu et al. (2010) developed an aPMV model and established the relationship between aPMV and PMV for Beijing, a city in China. Besides aPMV, Fanger and Tofum (2002) developed Extended PMV (ePMV) models for buildings without air conditioning and located in warm and humid climate zones.

The above-mentioned studies were merely a part of different adaptive models. Theses adaptive models provided many types of thermal comfort models for different types of environments which expanded the thermal comfort theory into a border filed. However, because the environments were different at every corner around the world, these models were usually only applicable for specific environments which limited their applications.

1.2.3.3 Psychological Models

The rational and adaptive models were both models that focused on environmental parameters such as air temperature and air velocity. However, the thermal interaction of human with the environment also involved psychological responses and physiological responses. Therefore, researchers developed models following these two approaches to further understand thermal comfort.(Cheng et al., 2012).

According to Guan et al. (2003) the psychological models did not describe the mental status in a thermal environment but predicted the local and whole-body thermal sensation. Taniguchi et al. (1992) related the average facial skin temperature and its changing rate to the whole-bod thermal sensation for vehicles. The model was developed based on human subject tests. This model only related the facial sensation with the overall sensation. Therefore, the model was not comprehensive enough. Hagino and Junichiro (1992) also conducted experiment in vehicle to determine the relationship between thermal sensation of whole body and thermal sensation of partial body

segment. The model reveled that the forehead and upper arm contribute the most to the whole-body sensations than thigh and instep. De Dear et al. (1993) proposed receptor model which applied different thermal sensation Area Summation Factors (ASF) to different regions base on sensitivities towards thermal stimuli. This model only represented local skin temperature and did not have enough information for whole-body thermal sensation. Wang (1994) developed a model to calculate the thermal sensation under transient conditions. It combined PMV model with an extra term which described the rate of heat storage in skin. This model provided a quick method to predict transient thermal comfort but it lacked the information of local thermal sensation. Kohri (2002 and 2003) defined the local-standard effective temperature with the dispersed two-node model to evaluate thermal environment at different body parts. Lomas et al. (2003) used large amount of experimental data of overall TSV to develop a Dynamic Thermal Sensation. This model had an expression as equation 1.1.

$$\mathrm{DTS} = 3 \times \tanh\left[a \cdot \Delta T_{sk,m} + F_2 + \left(0.11 \frac{dT_{sk,m}^{(-)}}{dt} + 1.19 \frac{dT_{sk,m}^{(+)}}{dt_{\max}} e^{-0.681t}\right) \cdot \frac{1}{1+F_2}\right] \tag{1.1}$$

$$F_2 = 7.94 \times \exp\left(\frac{-0.902}{\Delta T_{hy} + 0.4} + \frac{7.612}{\Delta T_{sk,m} - 4}\right)$$

In the equation, $\Delta T_{sk,m}$ and ΔT_h were the error signals of the skin surface temperature and the body core temperature. The derivative with respect of dt_{max} represented the maximum positive rate of change of the skin temperature.

These psychological models provided a more detailed information about the relationship between local thermal sensation and overall sensation. However, this study was not focused on this aspect. This approach was not further investigated in this study.

1.2.3.4 Physiological Models

The simplest physiological model was the empirical one-node model developed by Givoni and Goldman (1971). In their model, the considered the entire human body as one-node. However, this model was only applicable to hot environments. Gagge et al. (1971) developed a two-node model to evaluate thermal comfort. This model divided human body into two concentric cylinders with two different temperatures to represent core temperature and skin temperature respectively. This model provided a more detailed model to approximate heat transfer model for evaluating thermal comfort. This model had a wider application comparing to the one-node model. Another two-node model developed Azer and Hsu (1977) modified Gagge's two-node model and achieved a wider range of applicable environments. This model was able to determine thermal sensation directly from physiological strain. Later, Stolwijk (1971) developed a multi-node model to be used in aerospace applications. This model divided human body into six segments and each one was further divided into four layers in radial direction. Because the physiological phenomena of each section could be controlled, this model had better precision and flexibility than the previous ones. Even though this model was limited to steady-state conditions, it was regarded as the pioneer of modern multi-segment and multi-node physiological models. Fig. 1.1 shows the difference between single-segment and multi-segment model as well as the difference between two-node model and multi-node model.

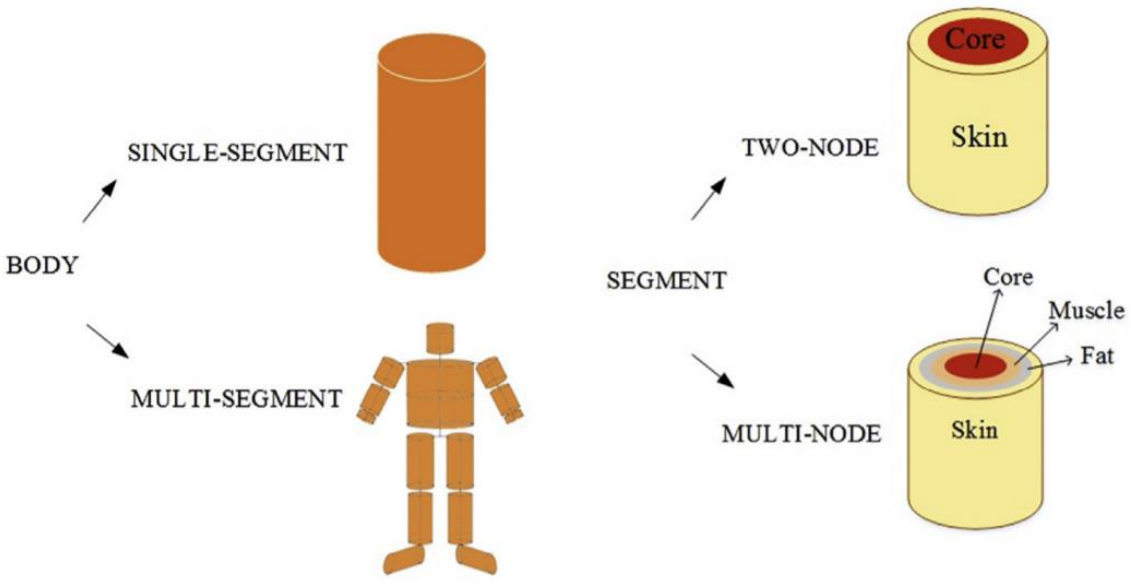

Figure 2.1 Comparison between physiological models (Katić et al., 2016)

Another physiological model was the UC Berkeley Comfort Model (Huizenga et al. 2001). This model could be applied to arbitrary number of segments, but usually used as 16 segments. For each segment, it was represented with multiple nodes to calculated heat exchange between each node. This model considered heat and moisture capacitance of clothing and heat loss by conduction to surfaces in contact with body, as well as improved convention and radiation coefficient. Individual differences such as body density, metabolic heat generation and blood flow rate were also considered in this model. Because of these improvements, this model could predict physiological response and estimate thermal comfort in transient or non-uniform thermal environments. Besides these models, the most complicated and realistic model was the multi-elements model that adopted finite element analysis (Li et al., 2004). This model solved differential equations to calculate temperature distribution of human body. Also, there were three-dimensional dimensional models that spitted human body into 15 cylindrical parts and used three thousand noes to represent human circulatory system.(Smith, 1991). This model was able to predict physiological responses of any local sections of human body.

These abundant physiological models provided a more detailed understanding of physiological responses toward thermal environment. It allowed scholars to make more accurate thermal comfort predictions by using this model. However, simple physiological models usually had worse performance than rational or adaptive models, and models with better performance were far too complicated. Due to this dilemma, the physiological models were normally used in theoretical analysis rather than experimental studies.

1.2.4 Physiological Indicators of Thermal Comfort and Measuring Instrument

The previous section discussed different types of models used to determine thermal comfort. Most of the models were either too complicated or only applicable to specific situations which limited their practicality. However, the physiological models inferred that human's physiological parameters would respond to different environments. Similarly, Harrison et al. (1988) concluded that human's thermoregulation system responds very quickly towards the change of outside environment. Another study (Wang and Peterson, 1992) also pointed out that when the environment was in the moderately warm (33.5 °C) to moderately cool (18 °C) condition, human's

thermoregulation system would vary skin temperature to maintain thermal comfort. These studies facilitated the effectiveness of using physiological parameters to determine thermal comfort.

Many studies have been conducted studies to find the most reliable indicative parameter. Jung and Jazizadeh (2018) adopted an optical technique called photoplethysmography to measure the blood volume change in microvascular bed of skin. The results showed 66.7% of the subjects showed a positive correlation between the vision indicators, skin temperature and thermal sensations. Another study conducted by Xiong et al. (2016) investigated behavior of different physiological parameters, including skin temperature at different locations, heart rate, etc. under the step change of air temperature. This study concluded that skin temperature was the most correlated parameter with thermal comfort. Yao et al. (2007) conducted experiment with 20 students participated to investigate three physiological parameters including skin temperature, electrocardiograph (ECG) and electroencephalogram (EEG) to see their responses to different air temperature. The study found that all of these were sensitive to room temperature and could indicate thermal sensation. Choi and Loftness (2012) investigated body skin temperature as an indicator of thermal comfort. Their study measured subjects' skin temperature at different locations using thermocouple and discovered the connection between wrist temperature and thermal comfort. Even though these studies investigated different physiological parameters, most of them concluded that skin temperature on forehead was the most indicative parameters about thermal comfort. Because skin temperature only dependent on the thermal status of human (Bierman, 1936) However, several other studies pointed out that measuring temperature at one point on forehead may not always be conclusive, for example Yi and Choi (2015) used thermographic camera to measure facial skin temperature and concluded that the facial skin temperature was five times more sensitive to ambient thermal conditions than other skin surfaces.

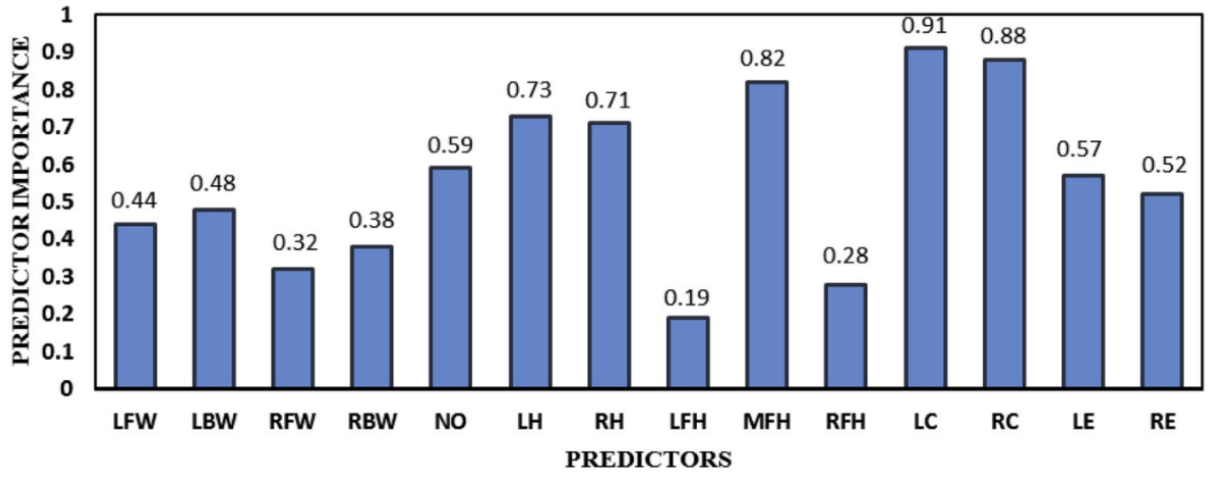

Figure 2.2 Correlation between facial skin temperature and thermal comfort (Salehi et al., 2020)

From fig. 1.2, Salehi et al. (2020) pointed out that the skin temperature of left cheek (LC) and right cheek (RC) has higher correlation with thermal comfort and the correlation was 0.91 and 0.88, respectively. Also, in their study, the skin temperature on middle of forehead (MFH) had a correlation of 0.82. In another experimental study of Li et al. (2018), the results showed that when the room was heated, the skin temperature of nose changed the most with 2.4 °C, the skin temperature of left cheek changed 1.1 °C and the skin temperature on forehead changed the least with 0.6 °C. From these studies, we could say that only using temperature on forehead was not always the best parameter to use. It would be better to use multiple skin temperature at different locations to predict thermal comfort. Therefore, because the face region is the least covered when a person is indoor, this study intended to investigate the relationship between averaged facial skin temperature and thermal comfort.

To measure and monitor occupant's physiological parameters, studies mentioned in previous section used either thermocouple or special equipment which were not ideal for occupants' daily life or for automatic operations. Recently, the development of wearable sensors for health monitoring provided non-invasive methods to measure physiological parameters. Liu (2018) used wearable sensors to measure physiological parameters to determine thermal comfort. Li et al. (2017) used the collected data from wearable sensors and a smart thermostat to build a random forest model for predicting thermal preference, and then used the model to determine the optimal room conditioning mode and HVAC setting via a smartphone. However, these wearable sensors

would also introduce an extra piece to the occupants and the accuracy of these sensors was not reliable.

On the other hand, thermographic camera was also able to measure skin temperature. Also, because the camera can be placed on surfaces, it introduced less interference than the wearable sensors. Thus, it was more ideal for applications. Cosma and Simha (2018) also used thermographic camera to measure local body temperature to model thermal comfort under transient conditions. Later, Cosma and Simha (2019) used the same equipment to develop a machine learning model to predict individual thermal preferences under transient condition. Wang et al. (2017) used online learned thermal comfort model using infrared thermal imaging to control the thermal environment. Li et al. (2018) used infrared thermography to measure temperature at different location on face and concluded that ears, noses and cheeks are the most indicative of thermal comfort and can reach an 85% prediction accuracy. Their experiment results showed that this system was feasible for actual application and effective for achieve more satisfactory indoor thermal environment using a smarter way. From these studies, they proved the reliability of the thermographic camera on measuring physiological parameters. However, their study only used such technology to model thermal comfort but did not modified the HVAC systems to trying to make occupants more thermally comfortable. Thus, this study intended to use thermographic camera to measure the mean facial skin temperature to determine occupant's thermal comfort and move one step further to improve the HVAC system to make occupants more comfortable.

1.3 Outline of this Thesis

In summary, this study developed and validated a new HVAC setpoint temperature control strategy for single-occupant office. The control strategy would provide a comfortable temperature setpoint for different clothing level determined by an image classification program. The control strategy would also adjust the temperature setpoint to meet occupant's thermal comfort need determined by mean facial skin temperature measured by long wave infrared (LWIR) camera combined with face detection program. To achieve this objective, this study conducted multiple investigations and reported them in following chapters:

Chapter 2 presents the development of the image classification model for measuring clothing level and the data collection for comfortable air temperatures. This study used an RGB camera combined

with the classification model to collect the data. The experimental data was used to determine the temperature setpoint for the new control strategy.

Chapter 3 presents the development of the thermal comfort model based on the mean facial skin temperature. The study used a LWIR camera combined with face detection program to collect mean facial skin temperature and corresponding thermal sensation vote (TSV). The model obtained was used to adjust the temperature setpoint in the new control strategy to meet occupant's thermal comfort need.

Chapter 4 presents the structure of the new control strategy implemented in LabVIEW by using results obtained from the previous chapters and discussed about the validation results of the new control strategy.

Chapter 5 summarizes the major findings of this study and discusses the possible future works.

CHAPTER 2. CLOTHING LEVEL CLASSIFICATION AND COMFORTABLE AIR TEMPERATURE

As stated in previous chapter, current setpoint temperature control did not consider occupants' clothing level which made people uncomfortable. Thus, this chapter aimed to develop an image classification model to determine clothing level as well as to determine the most comfortable temperature setpoint for different clothing level.

2.1 Clothing Level Classification

The first section talks about the development of the image classification model. Instead of building a new classification model, this study used a pre-trained CNN model and trained it again using the new dataset.

2.1.1 Pre-trained CNN Model

The first step was to search for available pre-trained CNN models. As mentioned in Chapter 1, CNNs have numbers of variations and it is impossible to decide which one is the best. Therefore, this study used CNN architecture called MobileNetV2 developed by Sandler et al. (2018). This architecture was specifically developed for mobile platforms where the computational power was limited. Different from other residual networks, this network used an inverted residual block to conserve the input information. The inverted residual block had a structure shown as Fig. 2.1. Normal residual block performed dimension reduction before doing the convolution, in this case, the original information would lose during the convolution. However, the inverted residual block first performed dimension expansion than did the convolution. By doing so, more information of the input could be preserved.

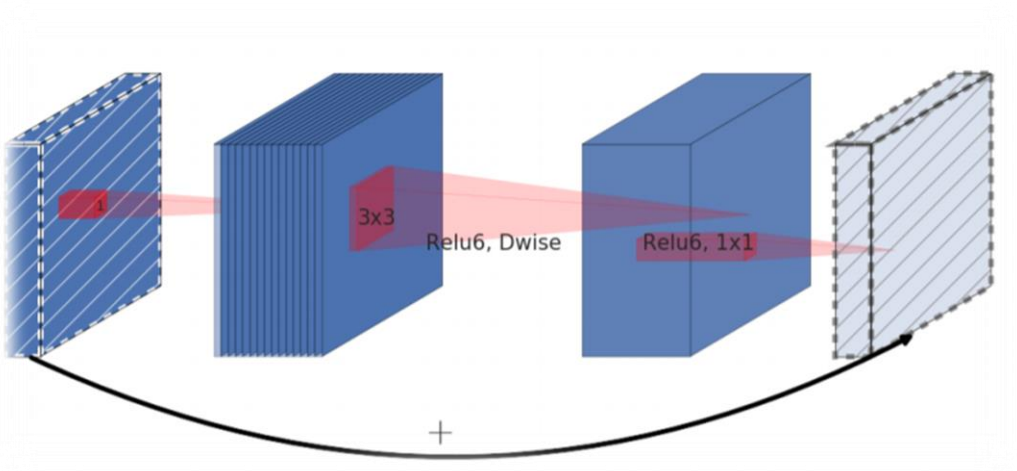

Figure 2.1 Structure of inverted residual block

Stacking different layers together, the model used in this study had a structure shown as Table 2.1. This model used 4 operators which are normal convolution with 3 × 3 kernel (conv2d), inverted residual block (bottleneck), normal convolution with 1 × 1 kernel (conv2d 1 × 1) and average pooling (avgpool). In the table, *c* stands for the number of output channels of each operator, *n* stands for the time the operator was repeated, s stands for the stride of the operator and *t* stands for the channel expansion factor applied on the input of each bottleneck operator.

Table 2.1 Structure of MobileNetV2

Input	Operator	t	c	n	s
$224^2 \times 3$	conv2d	-	32	1	2
$112^2 \times 32$	bottleneck	1	16	1	1
$112^2 \times 16$	bottleneck	6	24	2	2
$56^2 \times 24$	bottleneck	6	32	3	2
$28^2 \times 32$	bottleneck	6	64	4	2
$14^2 \times 64$	bottleneck	6	96	3	1
$14^2 \times 96$	bottleneck	6	160	3	2
$7^2 \times 160$	bottleneck	6	320	1	1
$7^2 \times 320$	conv2d 1x1	-	1280	1	1
$7^2 \times 1280$	avgpool 7x7	-	-	1	-
$1 \times 1 \times 1280$	conv2d 1x1	-	k	-	

2.1.2 Preparation of the Training Dataset

When preparing the dataset, this study applied following rules to build a clean and representative dataset: (1) The clothes should be fully visible including the shoes, since shoes also contribute to the total clothing level. (2) The color of the clothes should be various to avoid overfitting the classifier model with clothes color. (3) The height, weight, gender, etc., of the subject in the image should not be restricted to avoid overfitting as well. (4) The composition of the image should be simple (5) The subject in image should be standing out of background. Fig 2.2 shows examples of the dataset.

(a) (b) (c)

Figure 2.2 Sample images from retrain dataset: (a) 0.6 *clo* (b) 0.4 *clo* (c) 0.8 *clo*

The clothing level for each image in the dataset was manually calculated using method provided in the ASHRAE handbook (2009). The handbook instructed that the total clothing level of an ensemble was the summation of insulation value for individual garments. The insulation value was obtained from a table in the handbook and Table 2.2 shows part of the original table.

Table 2.2 Clothing insulation value

Garment Description[a]	$I_{clu,i}$, clo[b]	Garment Description[a]	$I_{clu,i}$, clo[b]
Underwear		Long-sleeved, flannel shirt	0.34
Men's briefs	0.04	Short-sleeved, knit sport shirt	0.17
Panties	0.03	Long-sleeved, sweat shirt	0.34
Bra	0.01	**Trousers and Coveralls**	
T-shirt	0.08	Short shorts	0.06
Full slip	0.16	Walking shorts	0.08
Half slip	0.14	Straight trousers (thin)	0.15
Long underwear top	0.20	Straight trousers (thick)	0.24
Long underwear bottoms	0.15	Sweatpants	0.28
Footwear		Overalls	0.30
Ankle-length athletic socks	0.02	Coveralls	0.49
Calf-length socks	0.03	**Suit Jackets and Vests (Lined)**	
Knee socks (thick)	0.06	Single-breasted (thin)	0.36
Panty hose	0.02	Single-breasted (thick)	0.44
Sandals/thongs	0.02	Double-breasted (thin)	0.42
Slippers (quilted, pile-lined)	0.03	Double-breasted (thick)	0.48
Boots	0.10	Sleeveless vest (thin)	0.10
Shirts and Blouses		Sleeveless vest (thick)	0.17
Sleeveless, scoop-neck blouse	0.12	**Sweaters**	
Short-sleeved, dress shirt	0.19	Sleeveless vest (thin)	0.13
Long-sleeved, dress shirt	0.25	Sleeveless vest (thick)	0.22

When calculating the clothing level for each image, the results were rounded to one decimal place to make distinguishable classes. Because, for example, the difference between 0.3 *clo* and 0.32 *clo* may be only a pair of socks. Thus, if the calculated results were not rounded, each class in the dataset would be very similar which made training the model very difficult and less efficient. Furthermore, this study considered all clothes worn by the person in the image were thin, because it was unlikely to judge the thickness purely based on the visual. Moreover, we assumed people would wear a T-shirt for ensembles with long-sleeved clothes. Similarly, underwear and socks were considered for all types of ensembles unless there were clear indications of not wearing these garments. Following these assumptions, the clothes worn by the man in Fig. 2.2(a) was approximated as follow: long-sleeved shirt, straight trousers (thin), underwear, T-shirt because he wore a long-sleeved shirt, shoes and socks. Therefore, the total clothing level for Fig. 2.2(a) was: 0.25 *clo* + 0.15 *clo* + 0.04 *clo* + 0.08 *clo* + 0.03 *clo* + 0.02 *clo* = 0.57 *clo* ≈ 0.6 *clo*. For Fig. 2.1(b) and 2.1(c), the calculated clothing level after rounding was 0.4 *clo* and 0.8 *clo*, respectively.

2.1.3 Training of the Image Classification Model

With dataset prepared, this study adopted the MobileNetV2 to build a new model for clothing level classification by using transfer learning. Transfer learning is a process that uses new dataset to modify a pre-trained neural network to solve new tasks. Fig. 2.3 illustrates the theory of transfer learning. In the figure, "knowledge" refers to the parameters and the architecture of the pre-trained network which would be preserved in the new network.

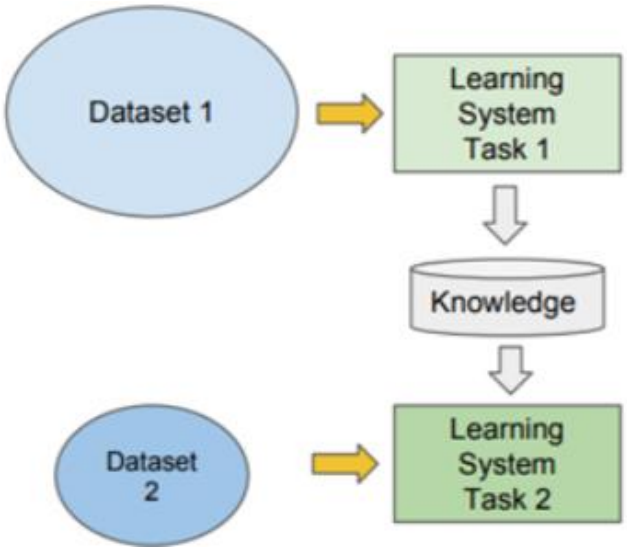

Figure 2.3 Illustration for transfer learning

Transfer learning not only saved time and but also required less computational power than building a new CNN model from scratch. This method could also preserve the performance of original network because the "knowledge" was not modified. However, since transfer learning uses the parameters and the architecture from other neural network, the performance of the retrained network is usually worse than the model built from scratch.

In this study, we connected a pre-trained MobilNetV2 with a linear classifier to build the clothing level classifier. Fig. 2.4 shows the structure of the classifier. By using this structure, we did not have to train the whole MobileNetV2 which had millions of parameters but just needed to train the linear classifier which had thousands of parameters.

Figure 2.4 Structure of clothing level classifier

With the structure determined, this study used Python as programming language and TensorFlow as the machine learning library to train the new model. The training program used cross-entropy as the loss function, and equation 2.1 shows the definition of it. In this equation, y stands for the one-hot encoding (Harris and Harris, 2012) for each class in the dataset and p stands for the predicted probability for each class.

$$L = -(y * \ln(p) + (1 - y) * \ln(p)) \tag{2.1}$$

For example, an image contained an object encoded as [0, 1, 0] and the prediction made by the classifier was [0.1, 0.8, 0.1] indicating that the classifier thought the object had 80% of chance being class [0, 1, 0]. Then, the loss for this image was $-(0 * \ln(0.1) + 1 * \ln(0.8) + 0 * \ln(0.1) = 0.223$. Because the value of loss function would be small when the prediction accuracy for the corresponding class was high, the goal to train the classifier was to minimize the loss function.

To minimize the loss function, this study used mini-batch gradient descent method. Mini-batch gradient descent was a method combing batch gradient descent and stochastic gradient descent. In batch gradient descent, the model was updated only after evaluating errors for all samples in the training dataset. This method could result in a more stable error gradient but a stable error gradient may lead to premature convergence of the model. On the other hand, in stochastic gradient method, the model was updated immediately after evaluating errors for each sample in the training dataset. This method could result in a better convergence but the computational cost was too high for larger datasets. Combining the ideas for these two methods, the mini-batch gradient descent first divided the training dataset into small batches (usually 32 samples per batch). Then, it updated the model after evaluating the errors for samples in one batch and move on to evaluate next batch. Therefore,

this method provided a more robust convergence than batch gradient descent and cost less computational power than stochastic gradient descent.

Table 2.3 shows the hyperparameters setting of the mini-batch gradient descent. The learning rate controlled the amount of updating the weight parameters in the model. The momentum was a constant value that would accelerates the training and avoid local minimum and the most common value for momentum was 0.9 (Smith, 2018). The batch size was the number of samples that would be used to update the model once. Also, a batch size of 32 was the most common setting (Smith, 2018). Lastly, the epoch means how many times the program trained over the full training group.

Table 2.3 Hyperparameters for mini-batch gradient descent

Hyperparameter	Value
Learning rate	0.0025
Momentum	0.9
Batch size	32
Epochs	60

After running the training program, it saved a model that could be used to perform clothing level classification. In this study, the model was tested using images captured from offices. If the classification model could predict most of the input images, then it would be reasonable to conclude that the CNN could be a feasible way to measure clothing level.

2.1.4 Results

The training dataset included 300 images for clothing levels ranged from 0.3 *clo* to 0.8 *clo* with increment of 0.1 *clo* which made a total of 1800 images. The images with the same clothing level were collected into the same folder and labeled with their clothing level. Fig. 2.5(a) shows the folders for different clothing levels and Fig. 2.5(b) shows part of the data for 0.4 *clo*. Because the training program assigned class labels by folders' name, the name of each image did not affect the training result.

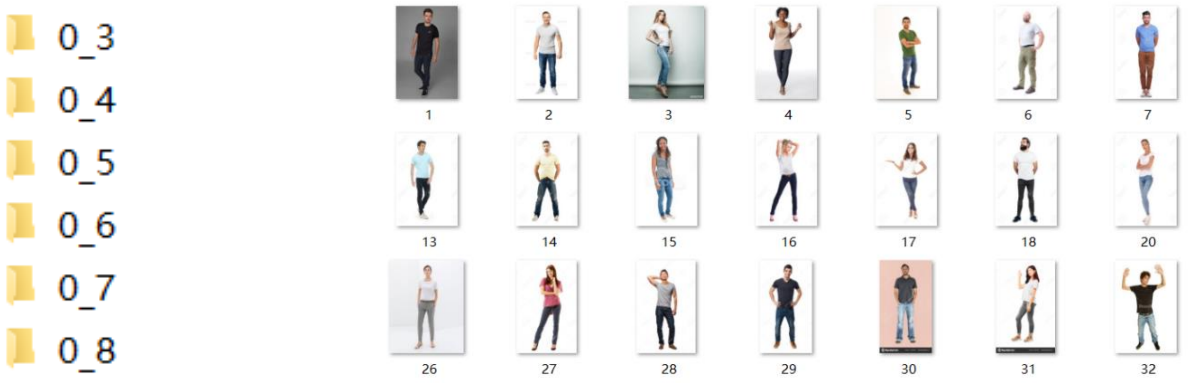

(a) (b)

Figure 2.5 Training dataset (a) Folders for different clothing level (b) Sample images for 0.4 *clo*

Fig. 2.6 shows the program successfully detected the images in different folders. The training program randomly separated the whole dataset into two sub-groups, one for training (1441 images, 80% of the dataset) and one for validation (359 images, 20% of the dataset). The training group was used to update the weight parameters in the classifier model and the validation group was used to evaluate the updated model. During the training, these two groups were kept independent with each other and the validation group were never used to update the model to avoid overfitting the model. Using the settings shown in Table 2.3, the 1441 training images was divided into 45 batches and 359 validation images would be divided into 11 batches. Therefore, for one training epoch, the model would be updated for 45 times and validated using 11 batches of images.

```
Found 359 images belonging to 6 classes.
Found 1441 images belonging to 6 classes.
Found 6 classes: 0_3, 0_4, 0_5, 0_6, 0_7, 0_8
```

Figure 2.6 Separation of the dataset

Table 2.4 shows the Python variable representation of the structure shown in Fig. 2.4. The *keras_layer* represented the MobileNetV2 which contained 2.2 million parameters. The program set these parameters to be non-trainable, following the theory of transfer learning. The *droupout* represented the Dropout layer. The Dropout layer could prevent overfitting by randomly disposing specific fraction of parameters in the model (Srivastava et al. 2014). This Dropout layer used 0.2 as the disposing rate. Also, the Dropout layer did not include any trainable parameters. The final

layer *dense* was the linear classifier including 7686 parameters that intended to be trained using the training dataset.

Table 2.4 Structure of the classifier in Python

Layer (type)	Output Shape	Param #
keras_layer (KerasLayer)	multiple	2257984
dropout (Dropout)	multiple	0
dense (Dense)	multiple	7686

Total params: 2,265,670
Trainable params: 7,686
Non-trainable params: 2,257,984

With the hyperparameters set to the values as shown in Table 2.3, the total training performed on a laptop consumed 4334 seconds. Fig. 2.7 (a) and (b) shows the average training loss and the average training accuracy for each epoch, respectively. In Fig. 2.7(a), the horizontal axis indicates the training epoch and the vertical axis indicates the cross-entropy value. The training had an initial loss as 1.69 and decreased to 1.2 at the next epoch. Then the loss started decreasing with a smaller rate until 50^{th} epoch. After the 50^{th} epoch, the training loss no longer had obvious change between consecutive epochs but damping around 0.68 in a range of 0.01, and the final training loss at 60^{th} epoch was 0.68. Based on the change of the loss, it was reasonable to say the loss function had converged after 50 training epochs. However, because the training dataset was small, it was unclear if the convergence reached a global minimum or fell into a local minimum.

In Fig. 2.7(b), the horizontal axis indicates the training epoch and the vertical axis indicates the training accuracy. Training accuracy indicated the how much data in the training dataset was correctly classified by the model. The initial training accuracy was 0.35 which was very low because the model was not well trained yet. The training accuracy increased to 0.59 at the next epoch. The trend of training accuracy was alike that of training loss but changing in a different direction. The training accuracy also reached a plateau at 50^{th} epoch which was like that of the training loss. The final accuracy at 60^{th} epoch was 0.92 and the averaged training accuracy was 85%.

(a) Average training loss for each epoch

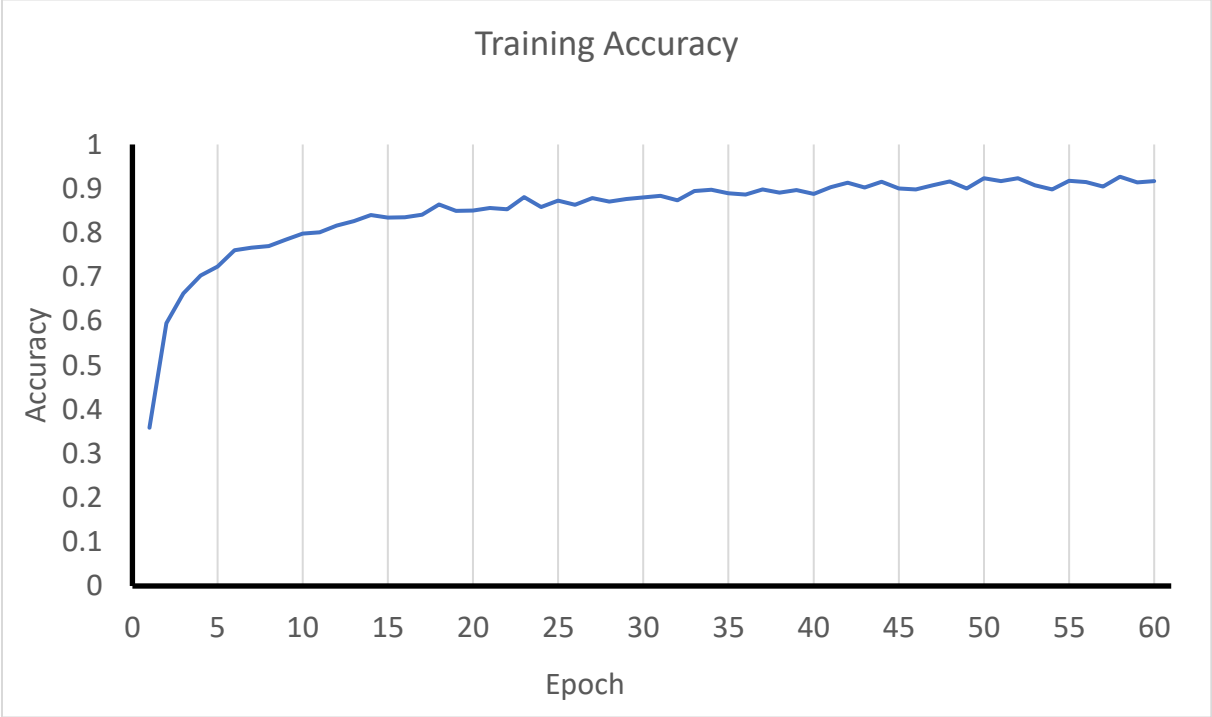

(b) Average training accuracy for each epoch

Figure 2.7 Results of training

Fig. 2.8 shows the averaged validation accuracy for each epoch. The horizontal axis indicates the training epoch and the vertical axis indicates the validation accuracy. The validation accuracy indicates how much data in the validation set was correctly classified by the classification model. The initial validation accuracy was 0.60 and increased to 0.70 at the next epoch. The training accuracy kept increasing until 8^{th} epoch. After 8^{th} epoch, the validation accuracy stopped increasing and damping around 0.74 within range of 0.1. After the whole training, the averaged validation accuracy for 60 epochs was 74%. This accuracy was acceptable given the size of the dataset.

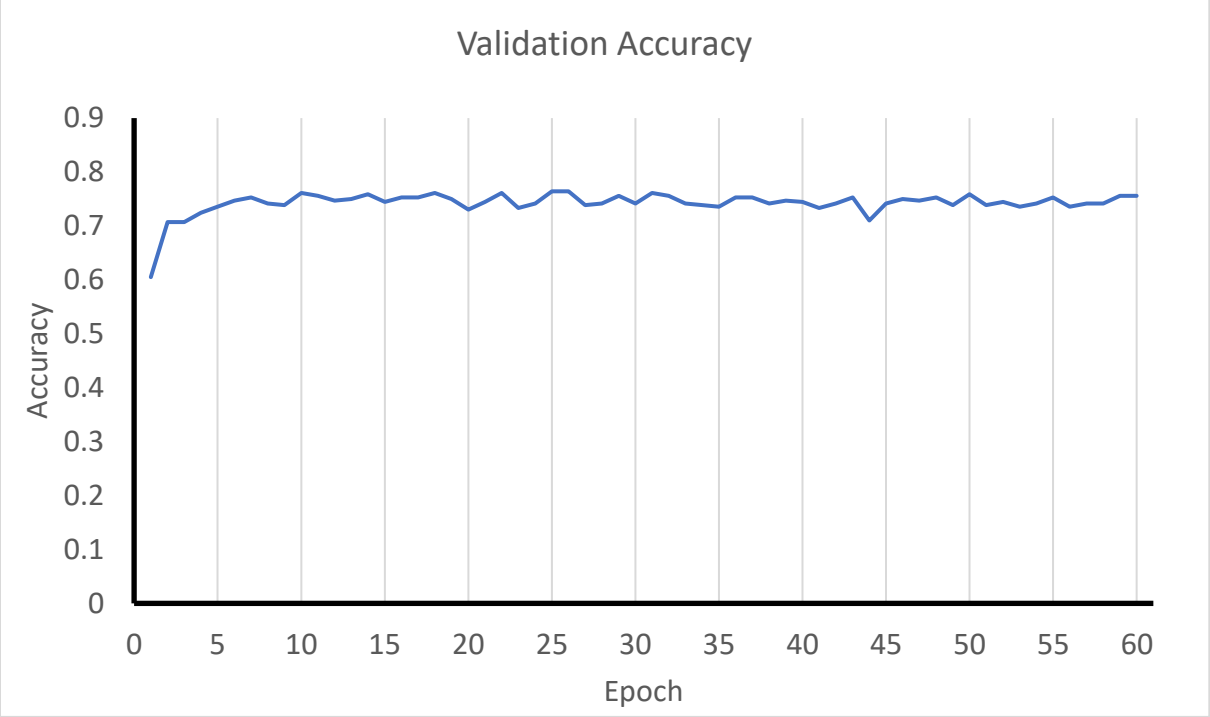

Figure 2.8 Average validation accuracy for each epoch

After the training, the model was tested using a new program to label 50 images captured from offices. Fig. 2.9 shows an example classification results using the trained model with different postures. In Fig. 2.9(b), the classifier had a level of confidence of 82% that the image had a clothing level of 0.3 and it did make the classification correct.

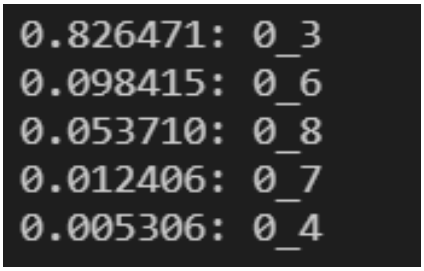

(a) (b)

Figure 2.9 Sample classification result (a) Input image (b) Classification result

Table 2.5 shows the overall classification performance of the 50 images. The classifier correctly classified 84% of the images and most of them were with high level of confidence. These results all showed that the CNN could non-invasively measure clothing level.

Table 2.5 Performance of the trained model

Result	Number of images
Correct (level of confidence > 70%)	35
Correct (70% > level of confidence > 50%)	8
Wrong	7

2.1.5 Discussions

This study investigated the method of measuring clothing level based on visual content using CNN. But the validation accuracy of the trained CNN model was not high enough. This was because that the CNN used in this study was not fine-tuned to this specific task. However, because fine-tuning the pre-trained CNN model would consume more computational power and more time as well as would require a more detailed dataset, the performance of a fine-tuned CNN model was not investigated. Furthermore, the trained model had a potential of overfitting because the dataset was small which limited the training effectiveness in each epoch. Normally, it would be ideal to train more steps in one epoch rather than training more epochs. Because the model would see the training data more times which increased the risk of overfitting the model with more epochs. Also, because the visual content for the same clothes could be very different in color, fitting and

materials, the dataset used in the training may not be comprehensive enough which may result in false predictions and overfitting. However, because it would be impossible to collect every kind of clothes in one dataset, there would always be some overfitting in every CNN models. Moreover, current CNN model could only measure clothing level for one person which limited its application in room with multiple occupants. Lastly, the CNN model was not good at telling the spatial information of an image, because the input was a 2-D image. Therefore, CNN could not tell if the subject was wearing a thick sweater or a thin sweater. Even though, it could be trained to classify thickness to some extent, the accuracy would still be low.

There was also a weakness of using the method mentioned in ASHRAE to calculate clothing level. Because the clothing level only reflected the total clothing level but did not considered the distribution of the clothes. For example, when a person wears a short-sleeved shirt, this person's arm would have a larger chance of cold/hot feeling than the torso parts. Using our method to predict clothing level could not reflect such uneven distribution of clothes. Therefore, it would be more ideal to determine the distribution to provide a more personalized environment.

2.2 Comfortable Air Temperature

As stated in the previous chapter, people with different clothes needed different air temperature to stay comfortable. Because there was no information available in existing literatures, it was our task to determine the comfortable air temperature for different clothing levels.

The experiment conducted in this study has been reviewed by Purdue University Institutional Review Board and received an exemption with protocol #1811021298.

2.2.1 Data Collection

This part of the study collected data on air temperature, clothing level, and thermal sensation in a single occupant office at Purdue University, U.S. The office was located on the second floor of a three-story building with the floor plan shown in Fig. 2.10 and the office had a layout shown as Fig. 2.11. The room had one side of exterior wall and the other walls were all interior.

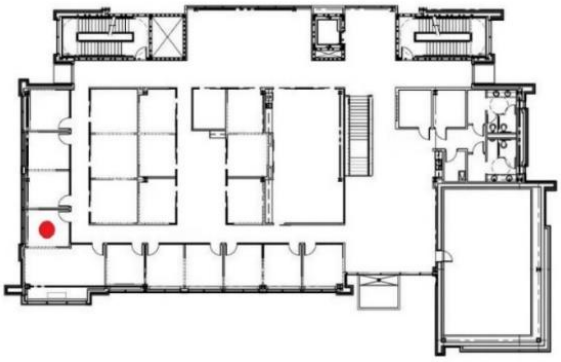

Figure 2.10 Location of the office, indicated by the red dot

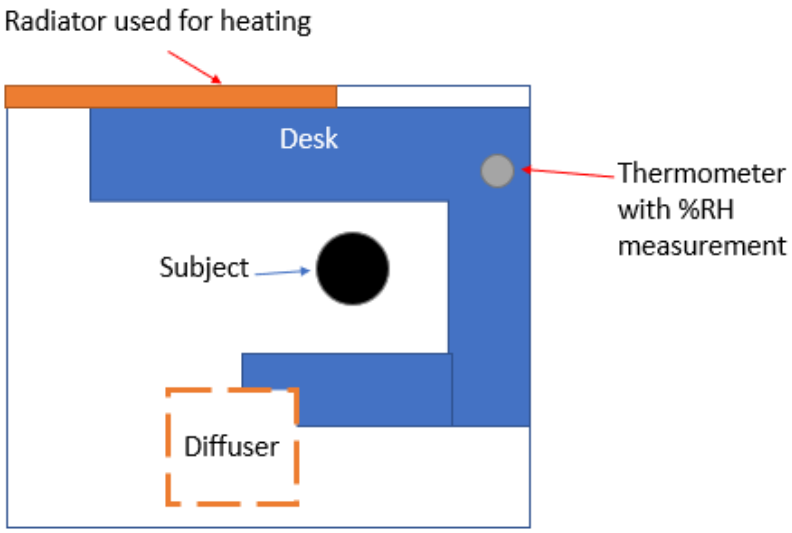

Figure 2.11 Office layout

This office used a thermostat (Siemens 544–760A) as shown in Fig. 2.12(a) which connected to building automation system (BAS) to control the room air temperature. The thermostat had an adjustment range from 18.3°C to 26.7°C. The data logger (Sper Scientific 800,049) as shown in Fig. 2.12(b) recorded the minute-by-minute air temperature in the office during the data collection. An RGB camera (Logitech C920) shown as Fig. 2.12(c) with a resolution of 1080p captured the occupant's images which were used for clothing level classification. To facilitate the clothing level classification result, we asked occupants to report their clothing level as well. If the self-reported clothing level was different from result of the classification program, we used the self-reported value as the true value. To understand the comfort of the subject, subject's thermal sensation was

recorded by questionnaires using the7-scale TSV (−3 for cold, −2 for cool, −1 for slightly cool, 0 for neutral, + 1 for slightly warm, + 2 for warm, and + 3 for hot) (ASHRAE, 2013).

(a) (b) (c)

Figure 2.12 Data collection devices (a) Thermostat (b) Data logger. (c) RGB camera

This study applied two assumptions and one restriction when collecting data: (1) The air velocity around occupants in the office was assumed to be below 0.2 m/s. If the air velocity was below 0.2 m/s, the effect of draft on the occupants was minimal. (2) The mean radiant temperature around the occupants to be the same as air temperature and the relative humidity in the offices to be between the comfortable range of 30% to 70% (ASHRAE, 2003). (3) The restriction was that all the occupants involved in the data collection were in sedentary state and performed office work during the investigation. Thus, their metabolism rate was at a similar level.

This study collected comfortable air temperature data for different clothing levels in the following procedure. Before the begging of the test, the subjects were instructed about how to report their thermal sensation using the seven-scale TSV. After the tutorial, we captured an image of the subject by using the RGB camera. We then input the image to clothing level classifier and recorded the classification result. Then, the subject entered the office with air temperature controlled to 20 °C. Subject spent 10 minutes after entered room for acclimation. This study used conclusion from Liu et al. (2013) to determine the acclimation time. They investigated the response of human thermal perception to step-change transient thermal environments. They concluded that subjects would be acclimated to the new environment after 10 minutes no matter how large the temperature changed. After the acclimation, we asked subject's TSV and increased the thermostat by 1 K if the subject felt cold or decreased by 1 K if the object felt warm. After the adjustment, we recorded subject's TSV and the corresponding air temperature every 2 minutes until the air temperature

reached the new setpoint. Then, if the TSV responded by the subject was still not comfortable, we repeatedly adjusted the thermostat according to the TSV until the subject responded TSV as 0. The air temperature at that time was regarded as the comfortable air temperature setpoint for subject's clothing level.

2.2.2 Results

This study collected more than 450 data points from college-aged participants for clothing level ranged from 0.3 *clo* to 0.8 *clo*. Fig. 2.13 shows the raw data collected from the experiment. The comfortable air temperature was different not only for different clothing level but also for different subject.

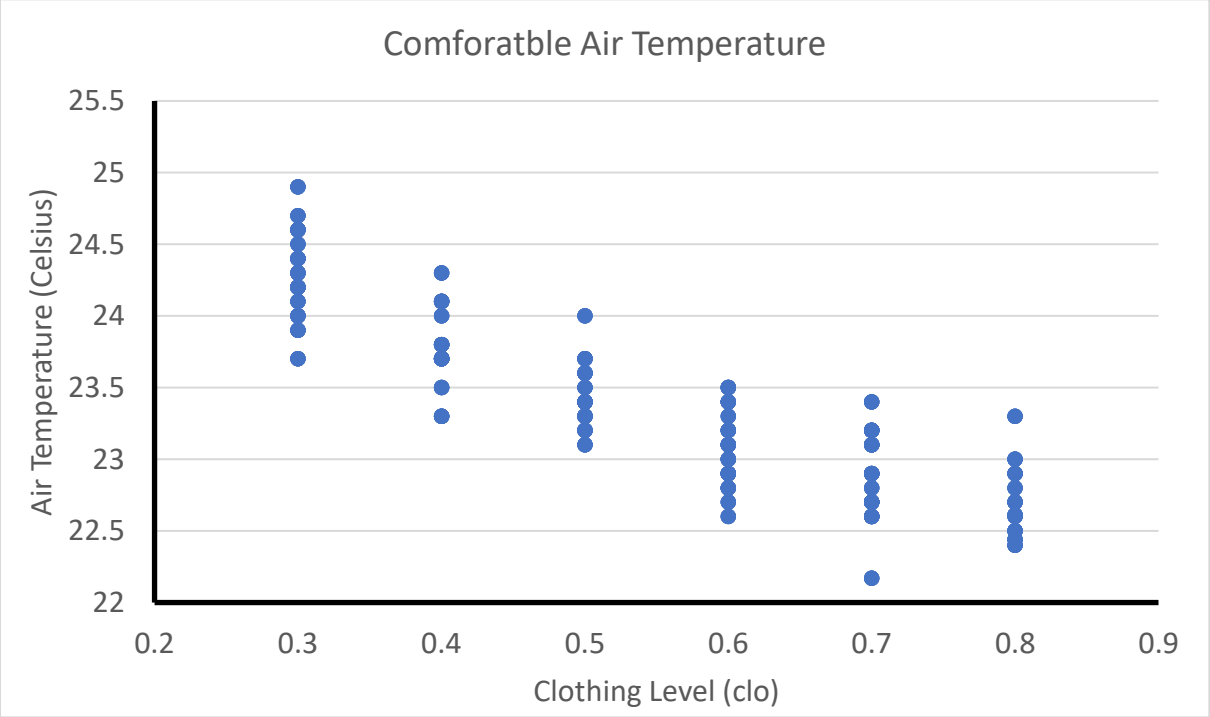

Figure 2.13 Raw data of comfortable air temperature

From the collected data, it was possible to determine a single comfortable air temperature for each clothing level. Therefore, the averaged air temperature at different clothing level was computed along with its standard deviation to examine the data distribution. Table 2.6 shows the calculation results. In the table, the mean air temperature shows that the comfortable air temperature increased as the clothing level decreased. When clothing level decreased, the area of skin exposed to the

environment increased which then increased the total amount of heat exchanged between human body and environment. Thus, the environment needed to be warmer to reduce the temperature difference between human and environment to preserve heat balance and maintain human's core temperature. Furthermore, the standard deviation was also calculated. Among each group, the standard deviation had similar magnitude. In the same group, the variation was small comparing to the average temperature. The maximum variation was 1.46% of average temperature for 0.4 *clo* and the minimum was 0.97% for 0.5 *clo*.

Table 2.6 Comfortable air temperature for different clothing level

Clothing Level (clo)	**0.3**	**0.4**	**0.5**	**0.6**	**0.7**	**0.8**
Average Air Temperature (°C)	24.3	23.8	23.4	23.1	22.8	22.6
Standard Deviation (°C)	0.29	0.34	0.23	0.29	0.33	0.24

Fig. 2.14 plots the averaged air temperature for different clothing level. The error bar in the figure has a value of 2 times of the standard deviation. This error bar could be regarded as the 95% confidence interval if we assume a normal distribution among each group. Even though the 95% confidence interval had overlap with each other, the averaged value still showed a clear trend. Based on the figure, it was reasonable to consider the air temperature as a dependent variable of clothing level. The datapoints were fitted with different type of trendline including linear, exponential, 2nd-order polynomial and logarithmic. These types of trendline could describe 96.2%, 96.5%, 99.9% and 99.6% of the variation of the average comfortable air temperature, respectively. The best fitted 2nd-order polynomial trendline had an equation as $y = 4.2185x^2 - 7.7836x + 26.239$ where y was the comfortable air temperature and x was the clothing level. By using this equation, it was possible to determine comfortable air temperature for any clothing level and use the calculated temperature as the temperature setpoint for the HVAC control system.

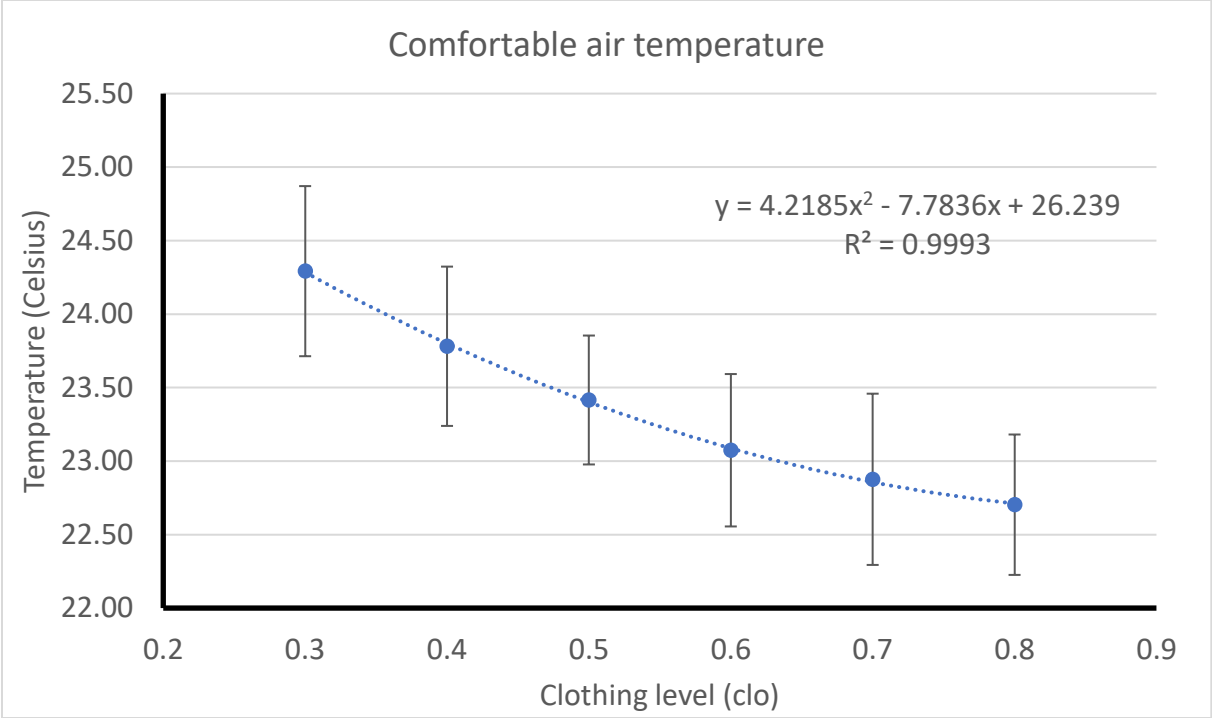

Figure 2.14 Second-order parabolic trend line for averaged comfortable air temperature

This study also calculated PMV and PPD using the experimental data to facilitate the findings. The PMV and PPD was calculated by using the tool developed by UC Berkley (Hoyt et al., 2019). This tool had an interface shown as Fig. 2.15. It automatically calculated the PMV and PPD based on the 5 inputs. Because this study assumed that the mean radiant temperature was equal to the air temperature, by using equation 2.2 the operative temperature calculated was the same as the air temperature. The equation was provided by ASHRAE Standard 55-2013. In the equation t_a is the air temperature, t_{mr} is the mean radiant temperature and t_o is the operative temperature.

$$t_o = \frac{t_a + t_{mr}}{2} \tag{2.2}$$

The air speed was set to 0.1 *m/s*, the metabolic rate was set to 1.1 *met* as if the occupant was doing office work, and the relative humidity was set to be 50% when validating each clothing level.

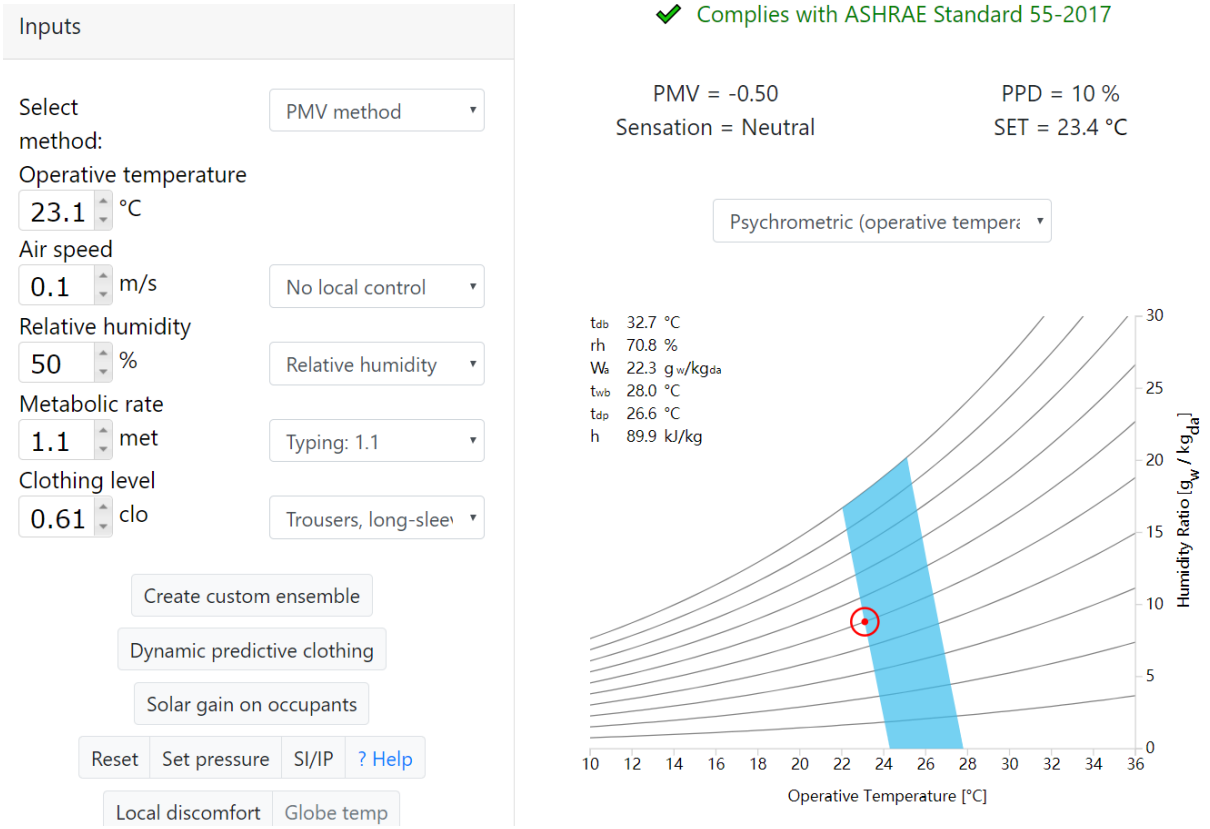

Figure 2.15 PMV calculation tool

Table 2.7 shows the calculated PMV and PPD using this tool. The calculated PMV was all negative indicating the air temperature was lower than the model required. The average PMV for 6 clothing level was -0.58. However, the absolute value for all clothing level was small, indicating a slightly uncomfortable environment. The PPD indicated the percentage of people that may feel dissatisfied under the given environment. The average PPD for 6 clothing level was 12.83%. The PPD had a maximum when clothing level was 0.3 *clo*. One reason that caused this large dissatisfaction might be the assumption that mean radiant temperature was the same as the air temperature. Because this clothing level was most common in summer and the outdoor air temperature was higher in summer. Because the office that used to collect data had one side of exterior wall, the mean radiant temperature would be higher than the air temperature in summer (Walikewitz et al., 2015). Therefore, the real operative temperature would be higher which would reduce the PPD. This reason could also be applied to 0.4 *clo* and 0.5 *clo* which were also common clothing level in summer. To validate the guess, we recalculated the operative temperature for 0.3 *clo* using mean

radiant temperature as 26 °C, then the PMV became -0.56 and PPD reduced to 12% improved from original calculation.

Table 2.7 PMV validation results

Clothing Level (clo)	**0.3**	**0.4**	**0.5**	**0.6**	**0.7**	**0.8**
Average Air Temperature (°C)	24.3	23.8	23.4	23.1	22.8	22.6
Calculated PMV	-0.86	-0.77	-0.66	-0.52	-0.4	-0.27
Calculated PPD	21%	17%	14%	11%	8%	6%

2.2.3 Discussions

This study investigated the comfortable air temperature for different clothing level. The overall trend was clear but the variation in each group was obvious which was reflected on the standard deviation. This variation was mainly due to the personal preference on thermal environment. Because thermal comfort was a personal feeling and this study did not asked subjects about their preference, these variations could not be explained by numerical analysis.

Also, the test group used in this experimental study was limited to college students, because they had easier access. Such bias on test groups would have impact on the results, because age had impact on both physiological and psychological. For example, for physiological, the metabolic rate of younger person would be higher than those of elderly which would make younger people felt cold less possible than elderly. Similarly, for psychological, younger person could had higher tolerance under cooler environment while elderly would prefer a warmer environment. Such source of error would have impact on the comfortable air temperature. Because for the same clothing level, younger person could report a lower comfortable air temperature than elderly. Therefore, conducing experiment with a test group with larger difference on age could improve the applicability of this model.

Furthermore, this study only asked about the overall thermal sensation of the subject but did not asked if subjects felt uncomfortable on specific body parts. Local discomfort had more effect on lower clothing level because the area of skin exposed to the environment would be larger than that of higher clothing level. With larger area of skin exposed, people would be more sensitive towards

air flow, air temperature change as well as the cold/heat radiance. Therefore, for lower clothing level, such as 0.3 *clo* or 0.4 *clo*, only controlling the air temperature may not be enough to optimize occupant thermal comfort, it would be ideal to investigate the presence of local discomfort.

In addition, rounding of the measured clothing level was also a source of variation for averaged comfortable air temperature. Because this process would over-simplify the population and increased the in-group differences. For example, the 0.4 *clo* in this study included clothing level ranged from 0.35 *clo* to 0.44 *clo*. The in-group clothing level had a 0.9 *clo* difference and it was reasonable to assume the comfortable temperature would be different for the clothing level on two ends. Therefore, it would be more informative and potentially reducing in-group variation if the population was divided into more detailed clothing levels.

2.3 Conclusions

This investigation trained an image classification model based on CNN to measure clothing level based on visual content and used it to investigate comfortable air temperature for different clothing levels. This study led to following conclusions:

(1) CNN based image classification could non-invasively measure clothing level with acceptable accuracy. Specifically, this study used MobileNetV2 and obtained an averaged training accuracy of 85% and an averaged validation accuracy of 74% without fine-tuning the model.

(2) People with different clothing level required different air temperature to stay comfortable. The comfortable air temperature could be calculated using equation: $y = 4.2185x^2 - 7.7836x + 26.239$, where y is the comfortable air temperature and x is the total clothing level.

(3) The air temperature calculated using this curve could provide an average PMV of -0.58 and an average PPD of 12.83%.

CHAPTER 3. MEAN FACIAL SKIN TEMPERATURE AND THERMAL COMFORT

Another objective of this study was to determine occupant's thermal comfort based on physiological parameters. Thus, this chapter aimed to investigate the relationship between mean facial skin temperature and thermal sensation. This study used LWIR camera to capture subject's thermal image of their face and then used a face detection program to locate the face to calculate the average temperature.

3.1 Face Detection

As discussed in Chapter 2, CNN was able to classify the class of an image. Also, CNN was able to detect face in an image. However, due to the large computational cost and complicated structure, this study decided to use another approach to perform face detection.

The other approach was to do face detection using Haar-like feature. Viola and Jones (2001) developed the Haar-like feature. They defined the Haar-like feature as "the difference between the sums of the pixel intensities in each region that are adjacent rectangular in a detection filter". Fig. 3.1 shows some filters with different shapes. With the filter placed at one location on the image, the Haar-like feature was obtained by subtracting the summed pixel value in shaded area from the summed pixel value in blank area.

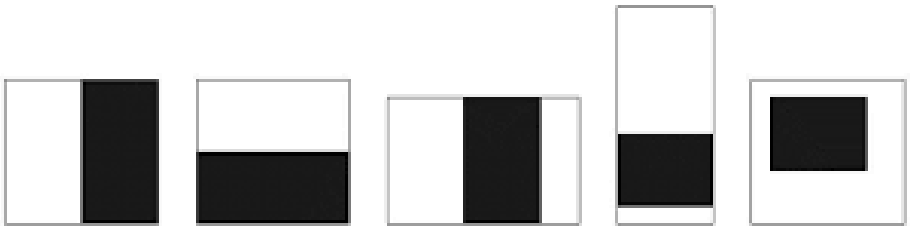

Figure 3.1 Different shapes of filters for calculating Haar-like feature

The advantage of Haar-like feature was the lower computational cost. Because, firstly, the input dimension of Haar-like feature was lower than that of the CNN. The Haar-like feature takes only grayscale image as input and the filters were usually two-dimensional (height and width) while CNN usually had a color image input and the filters were usually three-dimensional (height, width

and 3 color channels). This reduction in dimension reduced the times of calculating Haar-like feature. Secondly, calculating the Haar-like feature was faster than calculating convolutions. Haar-like feature was calculated using the summed-area table. In the summed area table, the value at any point (x, y) in the table was the sum of all the pixels above and to the left of (x, y), inclusive (Crow, 1984). For example, the sum of pixels of the shaded area in Fig. 3.2 can be calculated as $C + A - B - D$. This operation reduced computational cost to only four operations which was extremely less than calculating convolutions.

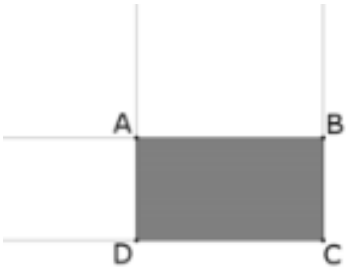

Figure 3.2 Calculating the sum of the shaded rectangle area

After calculating the Haar-features for different images, researchers found that human face share some common Harr-feature at specific location, for example, the region of the eyes was darker than the region of the cheeks. Thus, it meant the Haar-feature at these regions would be a special value. By using this special value, the Haar-feature could be used to detect human faces. However, using it was unlikely to find the face location by only calculating the Haar-like feature by once. Therefore, the process needed to be repeated to eliminate the false area in which the face was not presented. By eliminating all the false area, then the area remained would be where the face presented. Following this idea, the Haar-cascade model was developed and Fig. 3.3 shows the structure of the cascade model.

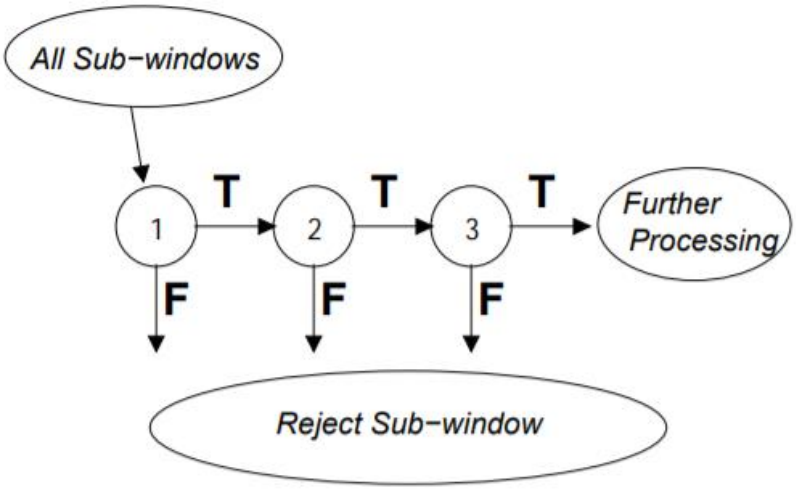

Figure 3.3 Haar-cascade face detection structure

This model first divided the input image into multiple small areas (sub-windows). In each small area, the model calculated the Haar-like feature and compared it with the threshold which represented the feature of human face. If the comparison result was in a specific range, the sub-window was labeled as true (represented as "T" in Fig. 3.3), and if the comparison result was not in the range, the sub-window was labeled as false (represent as "F" in Fig. 3.3). In the next step, the program would only perform Haar-like feature calculation in the sub-windows which were labeled as true in the previous step. Until the model found a region where all the sub-windows were classified as true, then this region would be regarded as the true location where a human face presented.

To implement this face detection, this study used Python as the programming language and OpenCV as the library. Because the Haar-cascade detection model was already available and it was a universal model, there was no need of training the model.

3.2 Temperature Measurement using Thermographic Camera

As discussed in Chapter 1, this study intended to use thermographic camera as a non-invasive way to measure the mean facial skin temperature. Hence, it was necessary to understand the working principle of the thermographic cameras before using it.

Thermographic camera was a type of a camera that did not capture visible light but captured infrared light emitted by objects. Everything that had a temperature higher than 0 K would emit infrared light (Herschel, 1800). The infrared light emitted by objects usually had a wavelength between 7 to 14 μm which was also known as long-wavelength infrared (Vollmer and Möllmann, 2011). Thus, the thermographic camera was also called as long-wave infrared (LWIR) camera. These LWIR cameras could measure the intensity of the infrared light emitted by an object using special sensors and processes the measurement with thermal radiation laws. Hence, the temperature of an object could be calculated.

There were two major types of LWIR camera, one was cooled cameras and the other was the uncooled cameras. As the name suggested, cooled cameras had a cooling system to cool the sensor. Such camera could reduce thermally induced noise and have a more accurate measurement, but the price was usually very high (FLIR, 2020). On the other hand, uncooled camera would have larger noise and less accurate result comparing to cooled sensors, but the price was lower and easier to operate. Therefore, due to cost limitation, this study used an uncooled camera to measure the temperature.

This study used Lepton 3.5 LWIR camera manufactured by FLIR. Fig. 3.4(a) shows the look of the camera. Because the camera core did not have ports to communicate with computer, the camera required an input/output (I/O) module to send the data to the computer. This study used a Purethermal 2 I/O module produced by GroupGets. Fig. 3.4(b) shows the I/O module with the camera mounted. The camera had a specification shown as Table 3.1, provided by the manufacturer. The camera was controlled by a program provided by the manufacturer which allowed user to read the camera status and perform calibration. Fig. 3.5 shows the user interface of the program. This camera had a nominal resolution of temperature measurement of 0.05 °C and a nominal accuracy that was less than 5%.

(a)

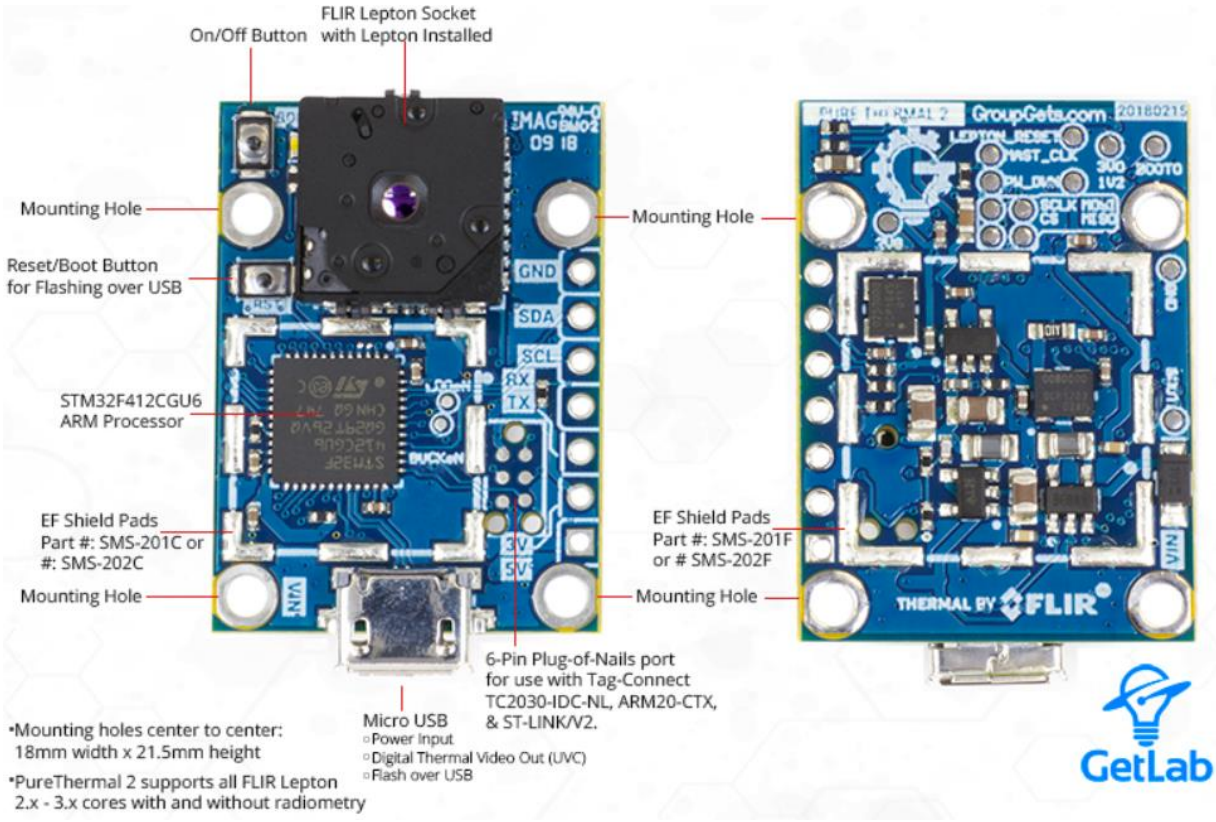

(b)

Figure 3.4 LWIR camera system (a) Thermal camera core (b) I/O module with camera mounted (GetLab, 2020)

Table 3.1 Specifications of Lepton 3.5 (FLIR, 2020)

Overview	Lepton 3.5
Sensor technology	Uncooled VOx microbolometer
Spectral range	Longwave infrared, 8 µm to 14 µm
Array format	160 x 120, progressive scan
Pixel size	12 µm
Effective frame rate	8.7 Hz (commercial application exportable)
Thermal sensitivity	<50 mK (0.050° C)
Temperature compensation	Automatic. Output image independent of camera temperature.
Radiometric Accuracy	High gain Mode: Greater of +/- 5° C or 5% (typical) Low Gain Mode: Greater of +/- 10° C or 10% (typical)
Non-uniformity corrections	Integral Shutter
Scene dynamic range	High Gain Mode: -10° to +140° C Low Gain Mode: -10° to +400° C (at room temperature) -10° to +450° C (typical)
Image optimization	Factory configured and fully automated
FOV - horizontal	57°
FOV - diagonal	71°
Lens Type	f/1.1
Output format	User-selectable 14-bit, 8-bit (AGC applied), or 24-bit RGB (AGC and colorization applied)
Solar protection	Integral

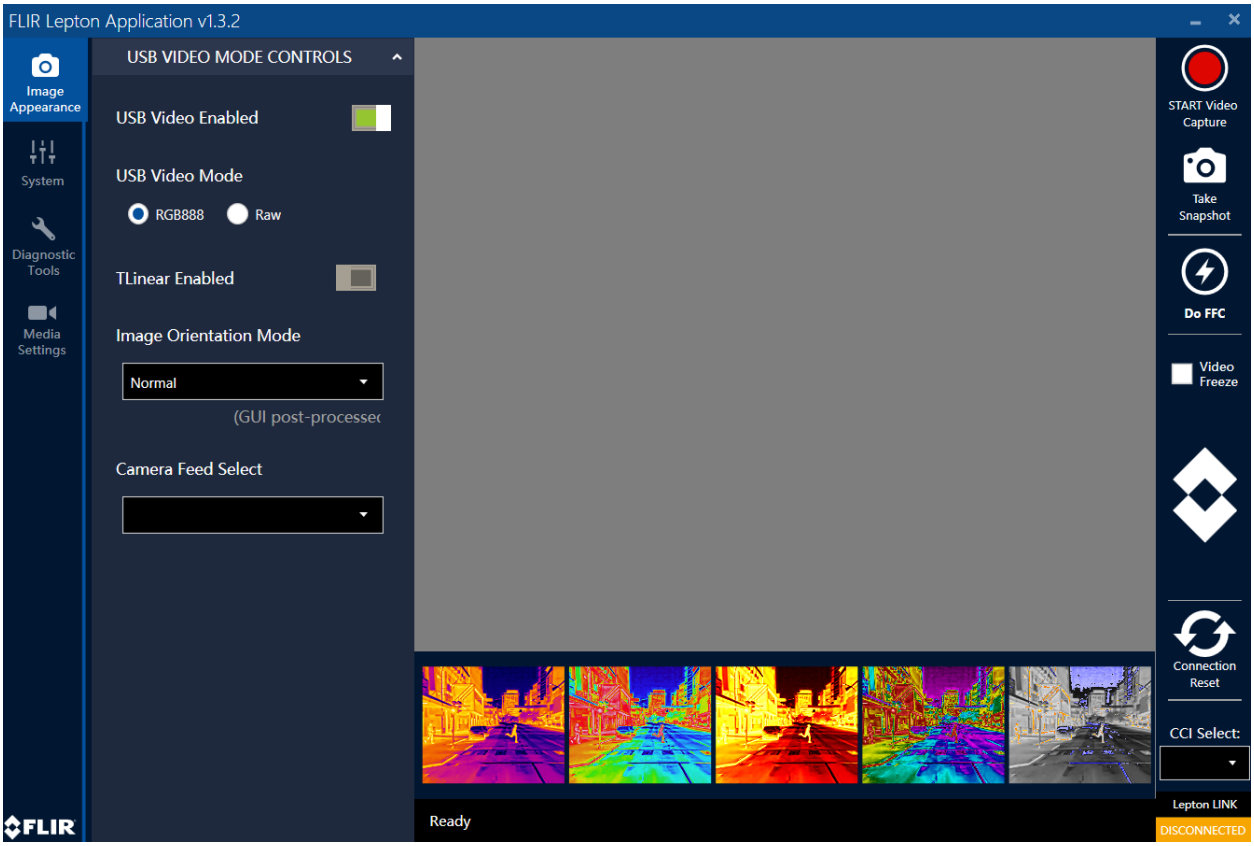

Figure 3.5 User interface of camera control panel (FLIR, 2020)

3.3 Data Collection

As stated in the Chapter 1, this study intended to investigate the relationship between mean facial skin temperature and thermal comfort. Thus, this part of the study collected data on air temperature, mean facial skin temperature, and thermal sensation in a single occupant office at Purdue University, U.S. The office was the same as the one discussed in Chapter 2 as well as the datalogger for air temperature measurement and the thermostat.

This study used the LWIR camera combined with the Haar-cascade face detection program discussed in the previous sections to measure the mean facial skin temperature. Because the skin temperature only dependent on the thermal status of human (Bierman, 1936), it was not necessary to collect the clothing level or air temperature. This study used the same questionnaire as the one in Chapter 2 to record occupant's thermal sensation. Assumptions and restrictions mentioned in previous chapter were still applicable to this data collection.

This study collected the mean facial skin temperature under different air temperature following this procedure. Before the begging of the test, the subjects were instructed about how to report their thermal sensation using the seven-scale TSV. After the tutorial, subject entered the office with air temperature controlled to 18 °C. Subject spent 10 minutes after entered room for acclimation. After the acclimation, we asked subject's TSV and captured the thermal image of subject's front face to measure the mean facial skin temperature. First, we controlled the air temperature in test office to be 23 °C to produce a neutral sensation. After a subject entering the office for 10-minute acclimation, we measured the mean facial skin temperature of the subject and asked the subject's TSV at that moment. Then we changed the thermostat setpoint by 1 K and recorded the corresponding mean facial skin temperature and TSV every 5 minutes. For each measurement, three thermal images were captured. During the experiment, this study managed the air temperature from 20 °C to 26 °C to produce TSV varied from -2 to 2 for every subject. This study did not collect the data for TSV = 3 or TSV = -3. Because of the mean facial skin temperature was lower than that at TSV = -2, then subject's TSV = -3. The same method was applied for determining TSV = 3.

3.4 Results

This first section presents the results of the face detection program using images captured by the LWIR camera as well as the results of using the program to measure the mean facial skin temperature. The second section presents the results of data collected from the experiment.

The experiment conducted in this study has been reviewed by Purdue University Institutional Review Board and received an exemption with protocol #1811021298.

3.4.1 Face Detection and Temperature Measurement

Fig. 3.6 shows a sample image captured by the LWIR camera. The image was in 14-bit image in grayscale with tagged image file format (.tiff), therefore, it was in monochrome and did not show any color information.

Figure 3.6 Raw image of the LWIR camera

Because the face detection program was only applicable to 8-bit grayscale image, the raw output was converted in to 8-bit scale using equation 3.1. In 8-bit grayscale, each pixel value represented an amount of light which was an intensity information. Pixels in grayscale image were saved as 8-bit binary numbers which could be expressed from 0 to 255 in decimal. A decimal number 0 meant the weakest intensity in the image which was shown as black while a decimal number 255 meant the strongest intensity in the image and shown as pure white. The number among 2 boundaries would be shown as different level of gray.

$$8 - bit\ grayscale\ = 255 * \frac{Raw\ Value - Global\ Minimum}{Global\ Maximum - Global\ Minimum} \quad (3.1)$$

The conversion equation used is shown as equation 3.2, the global minimum was the smallest value in the original image while the global maximum was the largest value in the original image. The advantage of this equation was that it took its own value to construct contrast instead of using constant numbers, thus this equation was universally applicable to any kind of image.

This study used MATLAB script to perform the conversion. The MATLAB version was R2017b. Fig. 3.7 shows the actual code. The first line read the image using the *Tiff* function which was specifically for handling images with .tiff format. This function would create a tiff object available for later process. The second argument in the function indicated the status of the object which was readable('r') or writable ('w'). Line 2 read the tiff object and saved the data into a new variable. Since the script read the tiff object as unsigned 16-bit integer (uint16), it could not be calculated in MATLAB. Line 3 converted the uint16 to double precision number. Line 4 and 5 found the global maximum and global minimum in the image. The script used two max/min operations,

because the first operation only provided the max/min value in each column. Therefore, the second operation could find the global maximum/minimum. Line 6 and 7 performed calculation shown as equation 3.1. Line 8 saved the converted image into portable network graphics (PNG) format.

```
1 –  pic1 = Tiff('020.tiff','r');
2 –  n1 = read(pic1);
3 –  n=double(n1);
4 –  MAX = max(max(n));
5 –  MIN = min(min(n));
6 –  normfac=(n-MIN)./(MAX-MIN);
7 –  normal=uint8(round(normfac*255));
8 –  imwrite(normal, 'gray.png');
```

Figure 3.7 MATLAB script for 8-bit conversion

Fig. 3.8 shows the result of converting image shown as Fig. 3.5 to 8-bit grayscale. Comparing to the original image, the object in the original image became visible.

Figure 3.8 Image in 8-bit gray scale

By applying the Haar-cascade face detection program on the 8-bit grayscale image, it successfully located the face and enclosed the face with green rectangle. Fig. 3.9 shows a sample result. Besides enclosing the face in an image, the program also provided the location of the face by outputting the coordinates of the enclosing rectangle. For this image, the four output values of the face detection program are [43 19 63 70]. The first and second value represented the horizontal and vertical coordinate of the top-left vertex of the rectangle, respectively. The third and fourth value represented width and height of the rectangle, respectively. By using this information, we could locate the face area of the subject and calculate the average temperature in that area to obtain mean

facial skin temperature. The Haar-cascade face detection was effective on detecting face in an image.

Figure 3.9 Face detection result

According to FLIR (2020), the temperature data stored in the thermal image captured by the LWIR camera was 100 times of the real temperature represented in Kelvin. Therefore, the data was converted to Celsius using equation 3.2.

$$℃ = \frac{Raw\ data}{100} - 273.15 \quad (3.2)$$

Fig. 3.10(a) and (b) shows the data before and after unit conversion. The converted data was rounded to 2 decimals for a more meaningful result.

29558	29556	29579
29566	29575	29558
29579	29571	29571
29556	29584	29569
29594	29581	29579
29575	29603	29590

(a)

22.4300	22.4100	22.6400
22.5100	22.6000	22.4300
22.6400	22.5600	22.5600
22.4100	22.6900	22.5400
22.7900	22.6600	22.6400
22.6000	22.8800	22.7500

(b)

Figure 3.10 Temperature conversion results (a) Raw readings (b) Readings in Celsius

Before calculating the mean facial skin temperature, this study considered that the subject may or may not wear eyeglasses. Because eyeglasses' temperature would result in false results, this study used the following producers to eliminate the effects. First, we compared all temperature in the

enclosed face area with the threshold to obtain a Boolean map. In the map, the value larger and smaller than the threshold would be 1 and 0, respectively. By multiplying the Boolean map with the original temperature map, the temperature smaller than the threshold would be zeroed out. Finally, the mean facial skin temperature was obtained by calculating average of non-zero values. In this study, the threshold was 27 °C, because facial temperature for healthy human under normal condition would never be lower than this value. Also, the threshold could also be adjusted to determine the best value. This method could also eliminate other source of errors such as the hair temperature and the wall temperature appeared in the enclosed area.

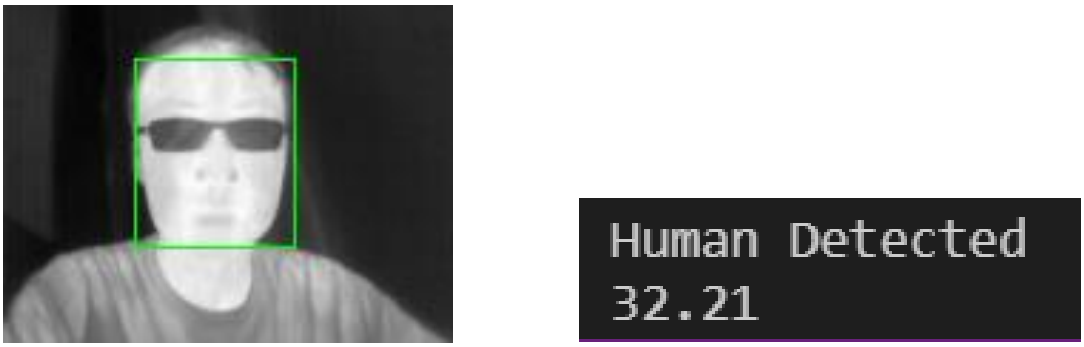

(a) (b)

Figure 3.11 Temperature calculation result (a) Detected face area (b) Calculated temperature

Fig. 3.11 shows a sample temperature result using images collected from experiment. Fig. 3.11(a) shows the enclosed face area and Fig. 3.11(b) shows the calculated temperature in Celsius. The processing time was 5 seconds for each image which was fast enough for real application. These results showed the effectiveness and practicality of combining LWIR camera and face detection program to calculate the mean facial skin temperature.

3.4.2 Mean Facial Skin Temperature and Thermal Comfort

After validating the LWIR camera and the face detection program, this study collected the data of mean farcical skin temperature and thermal comfort to investigate the relationship. Fig. 3.12 shows the collected data. The horizontal axis indicates the overall thermal sensation and the vertical axis indicates the mean facial skin temperature measured by the LWIR camera in Celsius.

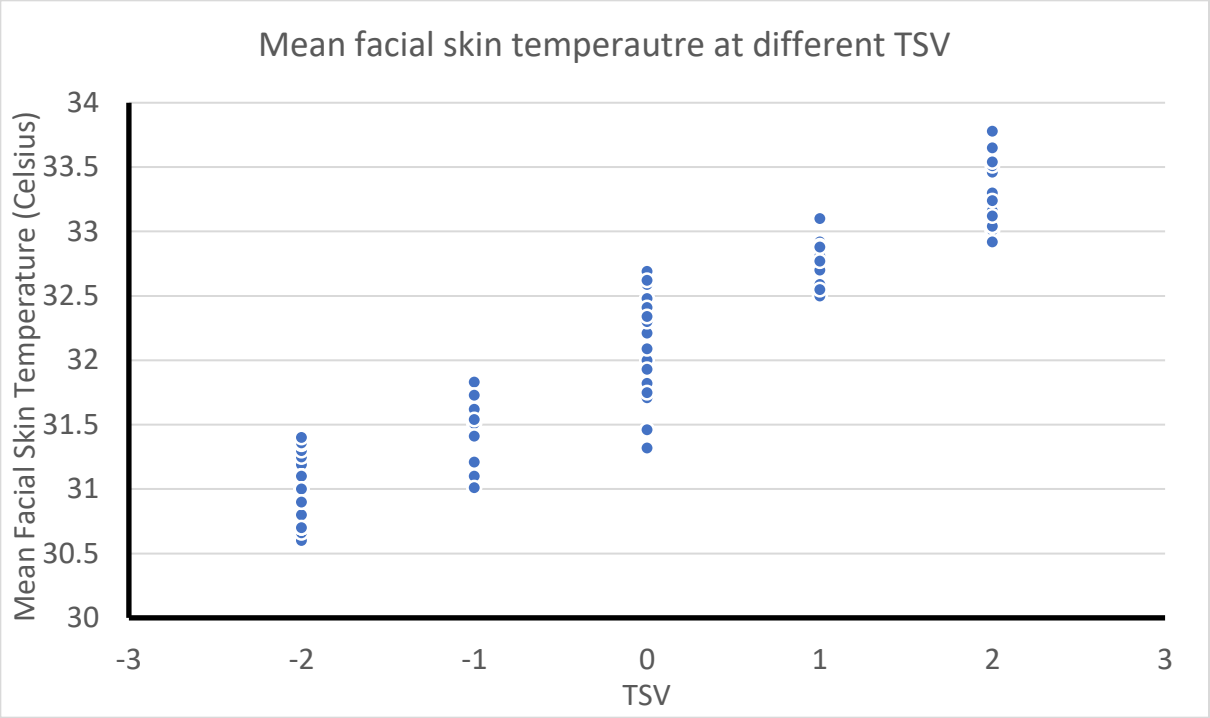

Figure 3.12 Mean facial skin temperature at different TSV

This study collected 225 data points for TSV from -2 to 2 from college student participants. Under the air temperature from 20 °C to 26 °C, people felt neutral at the most time, therefore, TSV = 0 had the most data points. For other TSV, the number of data points were similar. The data showed a clear trend that as TSV increased which meant the occupant felt hotter, the mean facial skin temperature increased. When the TSV decreased which meant the occupant felt colder, the mean facial skin temperature decreased. The minimum recorded temperature was 30.5 °C for TSV = -2 and the maximum recorded temperature was 33.78 °C for TSV = 2. In group variation existed for all TSVs, because skin temperatures were regulated by thermoregulation system, individual physiological parameters such as age and gender.

Fig. 3.13 shows the average mean facial skin temperature at different TSV. This data was obtained by calculating the average temperature at different TSV. The horizontal axis indicates the TSV and the vertical axis shows the average temperature in Celsius. The vertical line at each data point indicates the 95% confidence interval for that TSV. The calculation of this interval assumed a normal distribution among each group. The span of the interval was the largest for TSV = 0, indicating a large variation in the individual mean facial skin temperature. On the other hand, the

span of the interval was the smallest for TSV = 1. This indicated a small variation in the individual measurement.

In the figure, each temperature interval at each TSV had some overlap. The most overlap existed between TSV = -1 and TSV = -2. The upper bound of TSV = -2 almost reached the average value for TSV = -1. The least overlap existed between TSV = 0 and TSV = 1 as well as TSV = 1 and TSV = 2. For these three TSVs, there were no obvious overlap between each other. Such phenomena could be explained by the structure of human's thermoregulation system. In human thermoregulation system, thermoreceptors were used to sense cold and heat. When the environment temperature decreased, it would stimulate the cold receptors and send signal to brain to inform the presence of cold. When the environment temperature increased, it would stimulate the warm receptors and inform brain the presence of heat. However, because the location and numbers of these thermoreceptors, human's sensitivity to warm and cold was different. In human body, there were more cold receptors than warm receptors and the warm receptors located deeper in the skin than the cold receptors. Thus, people were more sensitive to cold than warm. In our study, because people were more sensitive to cold, people tend to report a lower TSV before their temperature dropped, which caused the large overlap for lower TSVs but not for higher TSVs. For example, a subject reported TSV = -1 at air temperature as 21°C, after 5 minutes, the temperature dropped by 0.2 °C but the subject reported TSV = -2. However, the mean facial skin temperature would not have big change with 0.2 °C difference in air temperature. Therefore, the mean facial skin temperature might not change but the TSV changed. Under TSV = 0 which was neutral sensation, the average skin temperature was 32.14 °C. By considering the 95% confidence interval which was 0.36 °C, the temperature range became from 32.5 °C to 31.78 °C. Based on these findings, it was possible to determine occupants' thermal sensation using mean facial skin temperature.

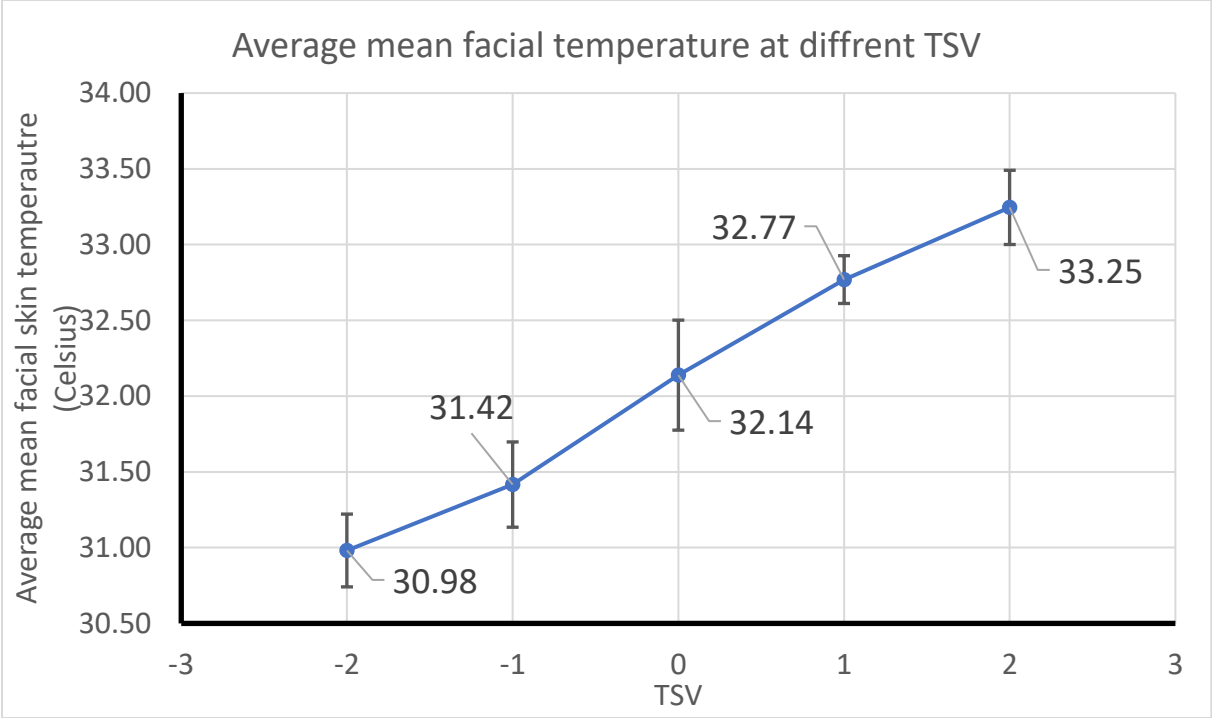

Figure 3.13 Average mean facial skin temperature at different TSV

This study also compared the results with other researcher's results shown as Fig. 3.14 (Choi and Loftness, 2012). In their results, it was obvious that the forehead temperature was proportional to thermal sensation. This trend was shared in their results and this study's results. However, in their results, the 95% confidence interval for each sensation vote was larger and had a lot of overlaps with other TSVs. The larger overlap would reduce the prediction accuracy in real application. However, in this study's results, the overlap was only obvious between TSV = -1 and TSV = -2. Hence, it was reasonable to conclude the mean facial skin temperature was more indicative than mean temperature on forehead.

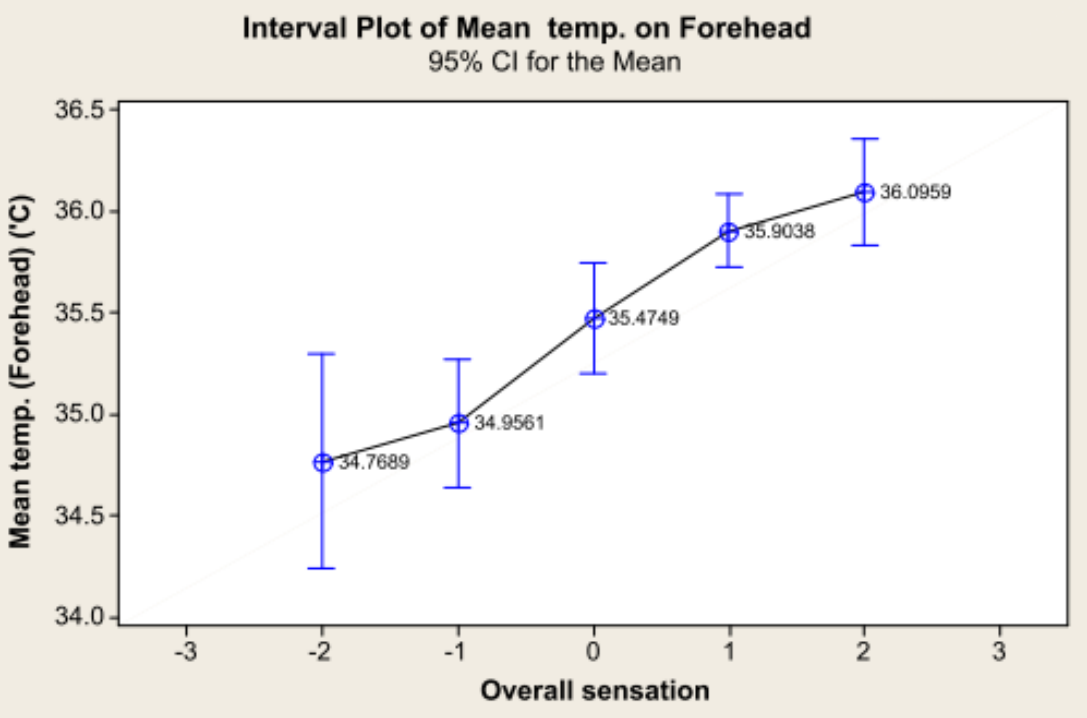

Figure 3.14 Mean temperature on forehead (Choi and Loftness, 2012)

3.5 Discussions

Human's thermoregulation system regulates our body temperature and it is the reason we experience cold or hot sensation. Even though different people have different preference and habit, all human should share the same trend. The trend would be that when environment temperature raised, people experienced hot sensation and our body temperature would raise, vice versa. In this study, subjects expressed similar trend of their thermal sensation and mean facial skin temperature. However, due to personal differences such as metabolic rate which affected heat generation of human body, there were inevitable inconsistency in response of skin temperature for different people. This inconsistency resulted in a relatively large confidence interval and would lead to the failure of our results. Also, like the previous experiment, the experiment conducted in this study used college students as major participants. Their TSV at different room temperature could not guarantee that everyone else would have a similar TSV. Therefore, in thermal comfort study, it was more likely to produce a model that perfectly suit one group of people rather than suit everyone. However, the model developed by using a larger number of subjects and subjects with different age would be more universal.

Another weakness of this thermal comfort study was the different understanding of TSV for different subjects. Even though this study provided instructions on how to report their TSV, it was still possible that the subjects reports TSV incorrectly. Because it was very difficult for every subject to have the same criteria for “slightly”. Such inconsistency introduced error for each TSV and compromised accuracy of predicting thermal comfort based on their mean facial skin temperature.

This study discovered another issue that was the location to measure air temperature. It was found that the air temperature at different location across the room had small variances. For example, if the air flow from diffuser had direct contact with the datalogger, the temperature reading would be different from the temperature the occupant was sensing. Therefore, it was another challenge to decide where to put the thermometer when performing this type of experiment.

Also, this study used thermographic camera to measure mean facial skin temperature. It worth to mention that the LWIR camera needed special care during the measurements. For example, in this study, the camera had a low resolution so it could not be placed further than 40-cm away from the subject. Otherwise, the subject’s face would be too small to be detected. Furthermore, during the study, it was spotted that the camera had a jump of reading after each calibration. But the reading became accurate after 2 minutes. Therefore, the measurement should be performed after 2 minutes of calibration.

3.6 Conclusions

This investigation combined LWIR camera with face detection program to measure mean facial skin temperature. By this approach, this study investigated the relationship between mean facial skin temperature and thermal sensation by experimental study. This study led to following conclusions.

(1) The mean facial skin temperature could be quickly and accurately obtained by the LWIR camera combined with face detection program. When subject felt comfortable, the mean facial skin temperature was between 31.78 and 32.5 °C.

(2) The mean facial skin temperature was more indicative than forehead temperature. For each sensation vote, the confidence interval for mean facial skin temperature was smaller than that of forehead temperature.

CHAPTER 4. IMPLEMENTATION AND VALIDATION OF THE CONTROL STRATEGY

This chapter describes the procedure and results obtained from field test in a single occupant office with the proposed control strategy, including comfortable air temperature setpoint determined by clothing level classification and automatically setpoint temperature adjustment based on prediction of thermal comfort by using the mean facial skin temperature.

4.1 Implementation of the Control Strategy

This study used LabVIEW 2018 to implement the control strategy. Fig. 4.1 shows the front panel (user interface) of the LabVIEW VI.

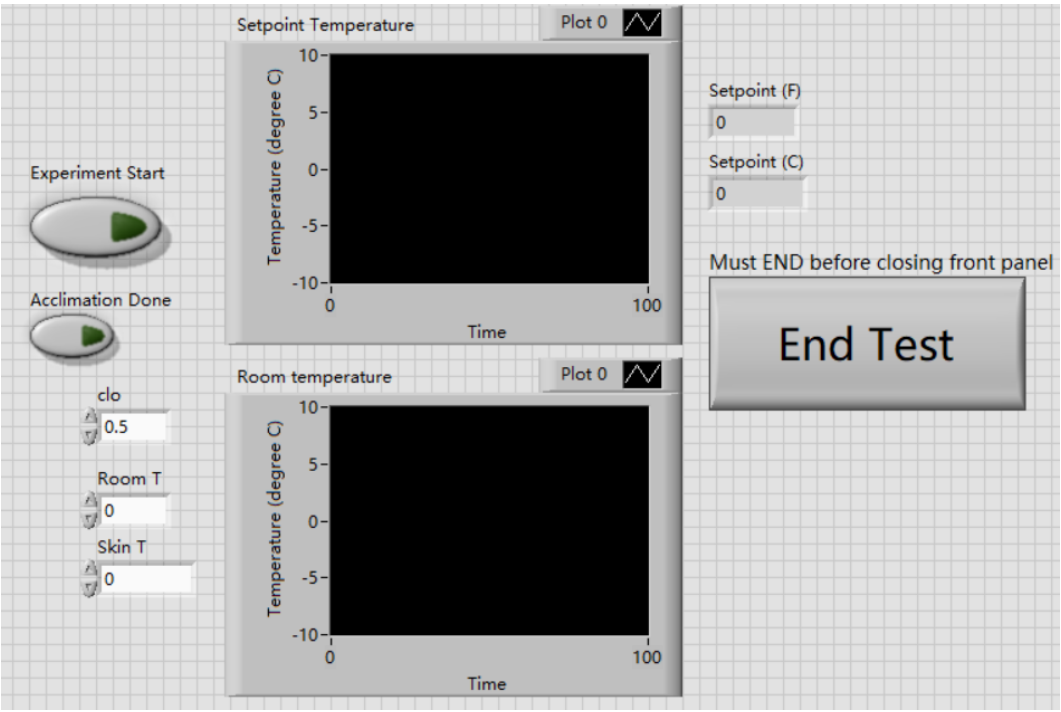

Figure 4.1 Front panel of the control system

There were three buttons that manage the infrastructure of control system and three inputs to perform the control strategy. Three buttons shown in the Fig. 4.1 are “experiment start”, “acclimation done” and “end test”. By triggering the “experiment start” button, it would enable the data communication between the sever machine where this VI was located and the BAS. Also,

it would disable local temperature setpoint control via thermostat. The “acclimation done” button would be triggered after the acclimation session which was the first 10 minutes of the experiment. Triggering this button would allow the program to change the static setpoint to a dynamic setpoint. The setpoint would be changing every 10 minutes based on the prediction result about occupant’s thermal comfort. The “end test” button would be pressed at the end of each test session to restore the system settings. It would reset the HVAC system in the room to the offset setpoint, terminate the communication between the server machine and the BAS and enable the local setpoint control via thermostat.

The control system also required three inputs to operate which were clothing level, room air temperature and the mean facial skin temperature. In Fig. 4.1, these inputs were represented as “clo”, “Room T” and “Skin T”, respectively. The first input, clothing level, was the value that described occupants’ clothing insulation quantitatively. This input was filled manually after running the clothing classification program described in Chapter 2. The second input, room temperature, it needed to be filled by hand based on the measurement obtained from the datalogger located by the subject. The third input, mean facial skin temperature, was also filled by hand using the value measured from LWIR camera using face detection program discussed in Chapter 4.

At current stage, these inputs were not automatically filled due to the hardware limitation and network structure. Hardware limitation referred to the circumstances that the fundamental hardware for the control strategy such as RGB camera, LWIR camera and the datalogger were operated on a personal computer. Because there were no I/O ports for the hardware, the data could only be obtained locally on the personal computer. Network structure of the server machine and the BAS also limited the automatic operation of the program. Because personal computer was not allowed to establish communication with the server machine due to security concern that adding a personal computer to a closed security network would make the network vulnerable to hostile attacks. Therefore, the inputs were currently filled manually but it would be possible to make them automatic if the hardware and network were specially designed for this control strategy.

Two graphs at the middle of the UI recorded and plotted the value of calculated setpoint temperature and air temperature every 10 minutes during the experiment. The data could also be saved as Excel spread sheet for later investigation. The setpoint temperature was in Celsius and it needed to be converted to Fahrenheit due to the requirement of the BAS.

The wiring diagram or the actual code of the control system is shown as Fig. 4.2. The outmost loop is the timed loop which is a discrete loop used for digital control. Inside the loop, it contains different input, output and communication functions and the structure at the center is the main code for control system. At the center of the loop, there is the function called case structure. Case structure is like an if statement that includes two instructions and each to perform based on the true or false condition of a Boolean input. In this case, the Boolean input is the “acclimation done” button representing the status of acclimation period.

Fig. 4.2 shows the wiring diagram of this VI. The outmost loop was the timed loop which was a discrete loop used for digital control. The loop was operated under 1kHz clock which provided a resolution of millisecond. The sampling period was set to 1 second. Because the control strategy only changed the temperature setpoint every 10 minutes, there were no necessity of using a faster sampling period. The other settings of the timed loop were set as default.

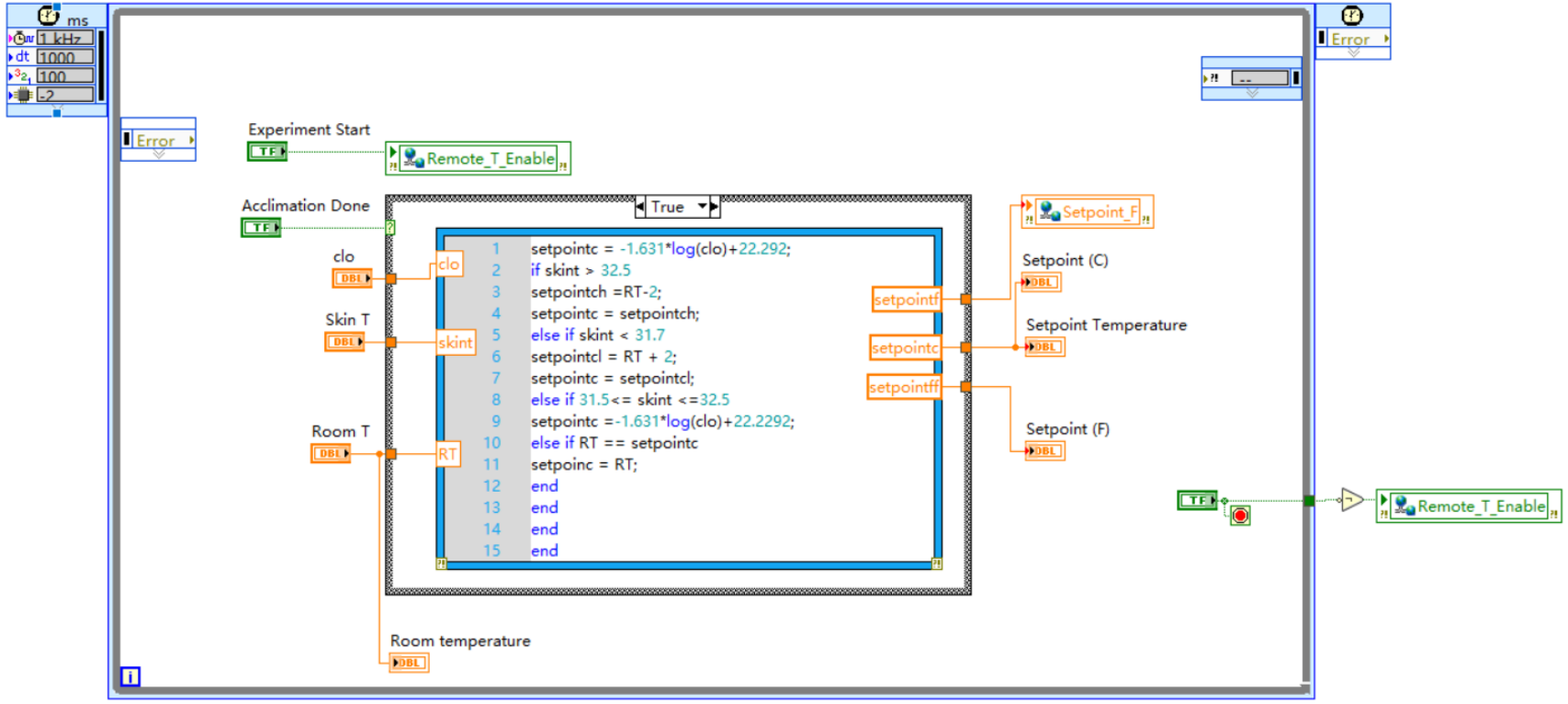

Figure 4.2 Block diagram of control VI

Inside the loop, it contained different input, output, communication functions and the structure at the center was the main code for control strategy. At the center of the loop, there was the function called case structure. Case structure was like an if statement that included two instructions and each to be executed based on the true or false condition of the Boolean input. In this case, the Boolean input was the “acclimation done” button representing the status of acclimation period. This study used Modbus protocol as the communication protocol to establish communication between the server machine and the BAS.

Acclimation period served as a buffer time for the occupant to eliminate the effects on thermal sensation due to their previous actives. Therefore, the setpoint temperature should be set to a constant during the acclimation period. Following this idea, Fig. 4.3 shows the script for setting the temperature setpoint during acclimation period. This study used MathScript node to calculate the temperature and unit conversion. The acclimation temperature setpoint was determined based on their clothing level, represented as “clo” in the figure, using the equation discussed in Chapter 2. This code also included the conversion between Celsius and Fahrenheit at line 2. After conversion, the setpoint was sent to the BAS.

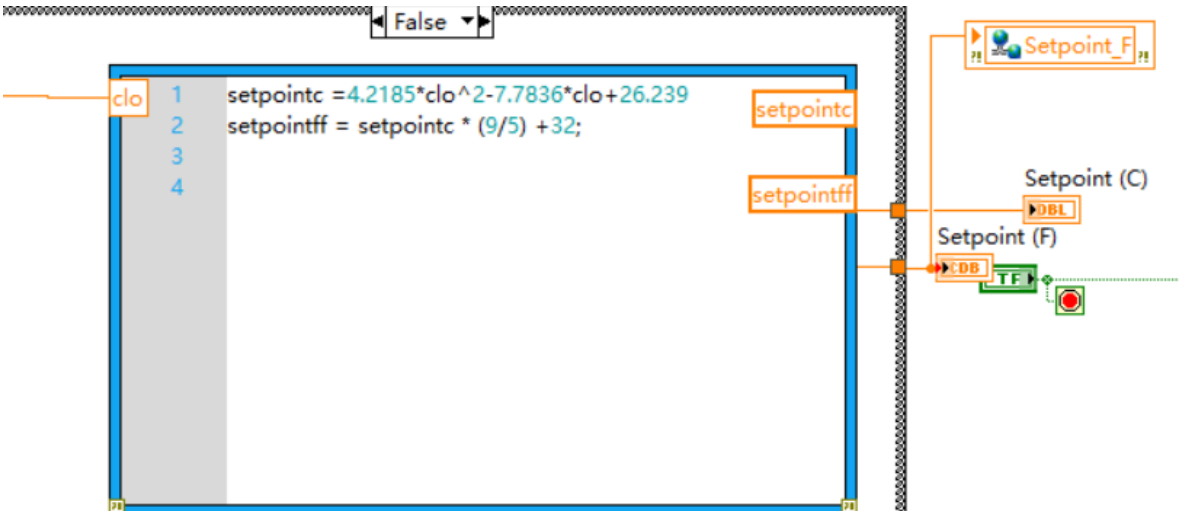

Figure 4.3 Control script for acclimation period

After acclimation done, the case structure would be triggered to true case. Under the true case, the setpoint temperature would be adjusted automatically every 10 minutes based on occupant’s mean facial skin temperature measurement. Table 4.1 shows the fundamental logic of adjusting the temperature setpoint. The decision of how to adjust the temperature setpoint was made based on

the results obtained from Chapter 3 that occupants felt comfortable when the mean facial skin temperature was between 31.7 and 32.5 °C. Therefore, when the mean facial skin temperature was lower than 31.7 °C, the setpoint would be increased by 1°C to raise the air temperature. When the mean facial skin temperature was higher than 32.5 °C, the setpoint would be decreased by 1 °C to reduce the air temperature. When the mean facial skin temperature was in-range, the setpoint was not changed.

Table 4.1 Fundamental logic for temperature setpoint adjustment

Mean facial skin temperature measurement (°C)	**Behavior of temperature setpoint**
Lower than 31.7 °C	Increase the setpoint by 1 °C
Higher than 32.5 °C	Decrease the setpoint by 1 °C
Between 31.7 and 32.5 °C (in-range)	Maintain at current setpoint

However, it was possible that the room temperature did not reach the temperature setpoint after 10 minutes and occupant still not felt comfortable. For example, at the first measurement the temperature setpoint was 21°C, the air temperature was 20.9°C and the mean facial skin temperature measured was 31.2°C. Based on this result, the temperature setpoint was adjusted to 22°C. After 10 minutes, the air temperature was 21.7°C and the mean facial skin temperature was 31.6. In this case, if we only used the decision table shown as Table 2.4, the temperature setpoint would be increased by 1°C again and the occupant may feel warmer after another 10 minutes because the air temperature may become too high. Therefore, it was necessary to compare the temperature setpoint and the air temperature before changing the temperature setpoint. Hence, the Fig. 4.4 shows the flowchart of the improved logic.

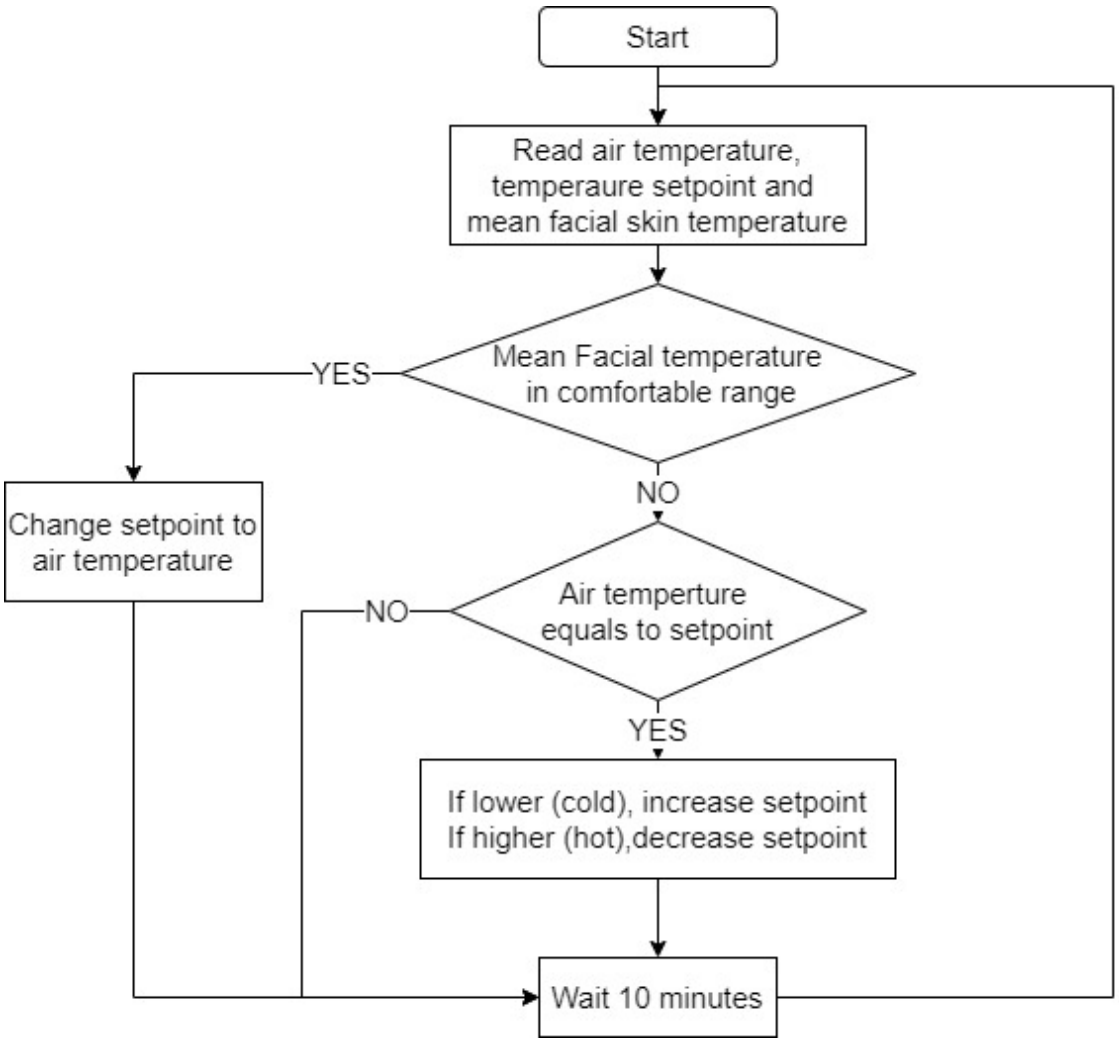

Figure 4.4 Flowchart of improved control logic

Based on the improved logic, the setpoint temperature was only changed if the air temperature was equal to the temperature setpoint. This logic also had an advantage that it could change the temperature setpoint to any value that occupant felt comfortable. For example, the temperature setpoint was 21°C, the air temperature was 20.9°C and the mean facial skin temperature measured was 31.4°C. After 10 minutes, the air temperature was 21.7°C and the mean facial skin temperature was 32.1°C. In this case, by using the improved logic, the temperature setpoint could be adjusted to 21.7°C rather than 22°C. This function could reduce occupant's overshoot on thermal comfort and may have a potential of energy saving.

Fig. 4.5 shows the implementation of the improved logic in LabVIEW. The function with an arrow and a star was the feedback node, it could send the value of the variable (setpointc) at previous

iteration. The program saved it as “cs” and compared with the room temperature to determine if the setpoint met the room temperature. Line 2 and 3 would reduce the temperature setpoint if the occupant felt hot and line 4 and 5 were for increasing the setpoint to warm the room up. Line 6 and 7 kept the setpoint the same as the room temperature. Line 11 was for unit conversion and send the setpoint to the BAS.

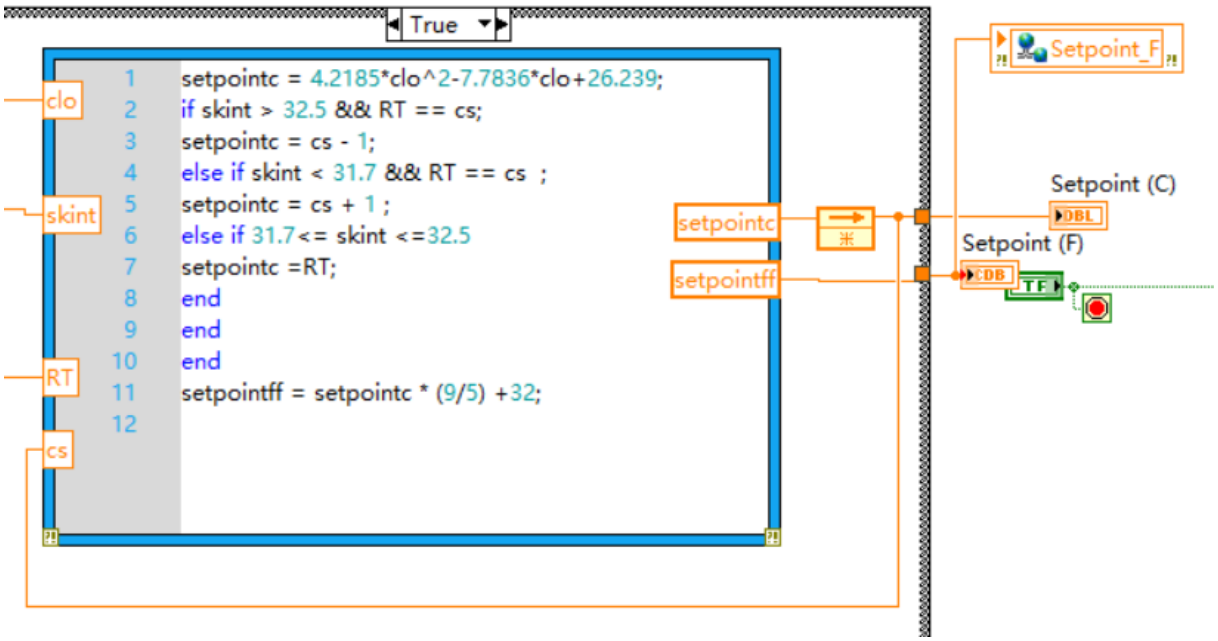

Figure 4.5 Implementation of improved control logic

4.2 Validation of the Control Strategy

After developing the control platform, this study performed validated our control logic and strategy. This study conducted validation in the same location as the one mentioned in Chapter 2 (shown as Fig. 2.10 and Fig. 2.11). The experiment used the same data logger to measure air temperature. This study also used the Lepton LWIR 3.5 camera and Logitech RGB camera for mean facial skin measurement and clothing level classification. We used the same questionnaire to collect subject’s TSV. The same assumption was also application to this experiment.

To collect the validation result, this study followed following procedures. Upon the arrival of subject, researcher first measured the clothing level of the occupant and input it to the control platform. The program sent the initial temperature setpoint to the BAS which controlled the test room air temperature to the setpoint. Subject would stay in another room until the temperature in

the test room reached the setpoint. Also, subject would be instructed how to report the TSV. Once the temperature met the setpoint, the subject entered the test room and began a 10 minutes acclimation period. At the end of the acclimation period, we measured the mean facial skin temperature and recorded the results into an Excel spreadsheet. The measured mean facial skin temperature and the room temperature obtained from datalogger was inputted to the control system. Then, the setpoint temperature of HVAC system would be adjusted accordingly following the improved logic. Meanwhile, subjects' attitude towards the thermal environment was also surveyed using the seven-scale thermal sensation vote. The survey results would help consolidating the method of predicting thermal comfort based on mean facial skin temperature. This set of measurement would happen every 10 minutes during the whole 60 minutes experiment. Therefore, the total time for one experiment session was 70 minutes including10 minutes acclimation session. During the experiment, the subject would perform activities involving minimum physical effort such as typing, reading, etc. to keep the metabolic rate at a constant and consistent value for different subjects. Also, for different subjects, their clothing levels were different but subjects were advised not to change clothing during the experiment.

4.3 Results

The experiment conducted in this study has been reviewed by Purdue University Institutional Review Board and received an exemption with protocol #1811021298.

This study performed 22 test sessions to validate the control strategy. Table 4.2 shows the summarized result of the 22 test sessions. There were three major types of the result. The type 1 results included tests that the subject felt comfortable through the whole experiment, this type of the results could prove the effectiveness of the comfortable temperature curve. The type 2 results included tests that the subject did not felt comfortable with the initial temperature setpoint but became comfortable again by adjusting the setpoint. This type of the results could prove the effectiveness of the thermal comfort prediction based on mean facial skin temperature. The type 3 results included tests that the subject did not felt comfortable by using this strategy.

Table 4.2 Number of tests for different types of the results.

Thermal sensation votes	Number of tests
Neutral (TSV=0) during the whole experiment	14
Initially uncomfortable (TSV≠0) with the setpoint then become comfortable (TSV=0) after changing setpoint with facial skin temperature	6
Uncomfortable (TSV≠0) with the control strategy	2

Fig. 4.6 shows a typical response of the type 1 result. Fig. 4.6(a) shows the air temperature, Fig. 4.6(b) shows the setpoint temperature, Fig. 4.6(c) shows the mean facial skin temperature and Fig. 4.6(d) shows the TSV. The clothing level of this subject was 0.3 *clo* and the temperature setpoint calculated was 24.3 °C. The horizontal axis for all figures stands for the time passed after acclimation period in minutes and the vertical axis stands for temperature in Celsius for temperature results and TSV for thermal sensation results.

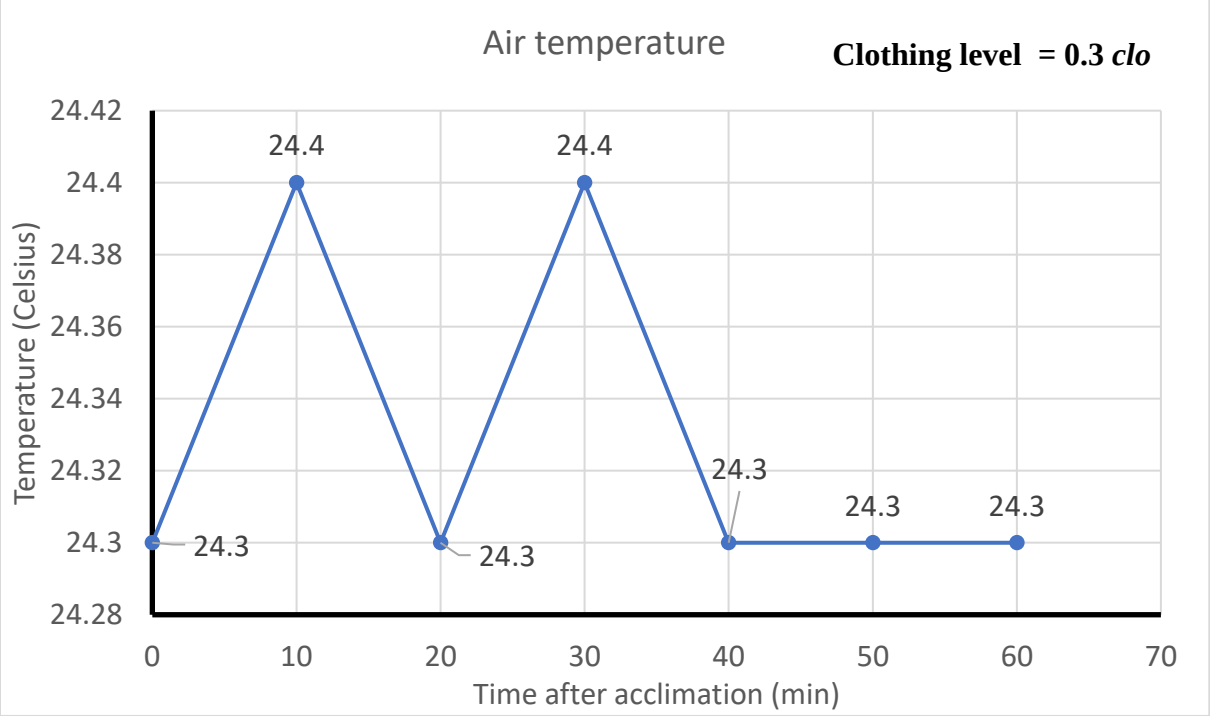

(a) Air temperature during the experiment

Figure 4.6 Type 1 sample results

Figure 4.6 continued

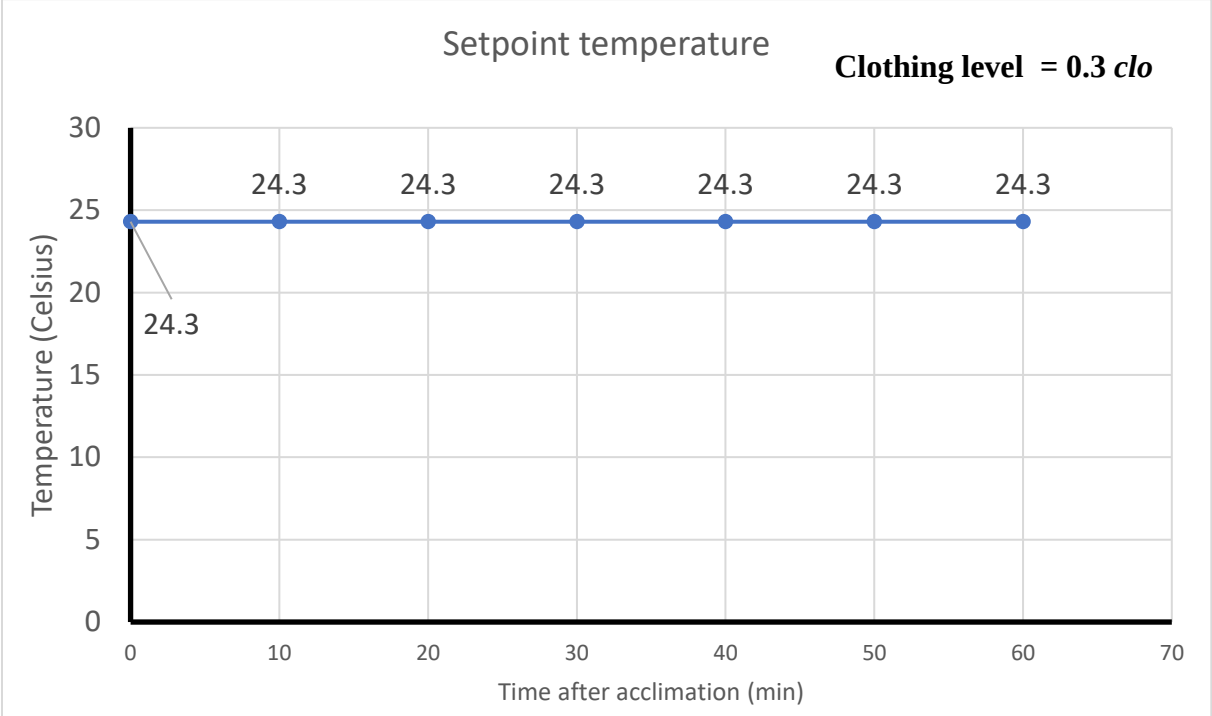

(b) Setpoint temperature during the experiment

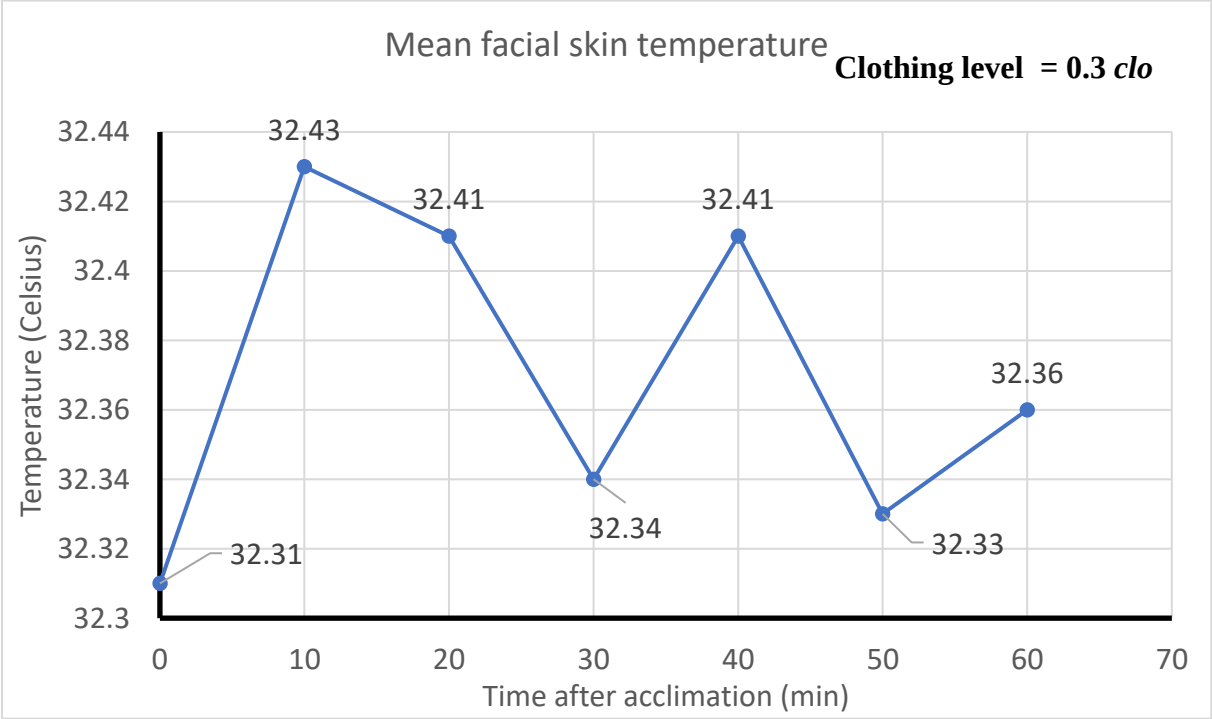

(c) Mean facial skin temperature during the experiment

Figure 4.6 continued

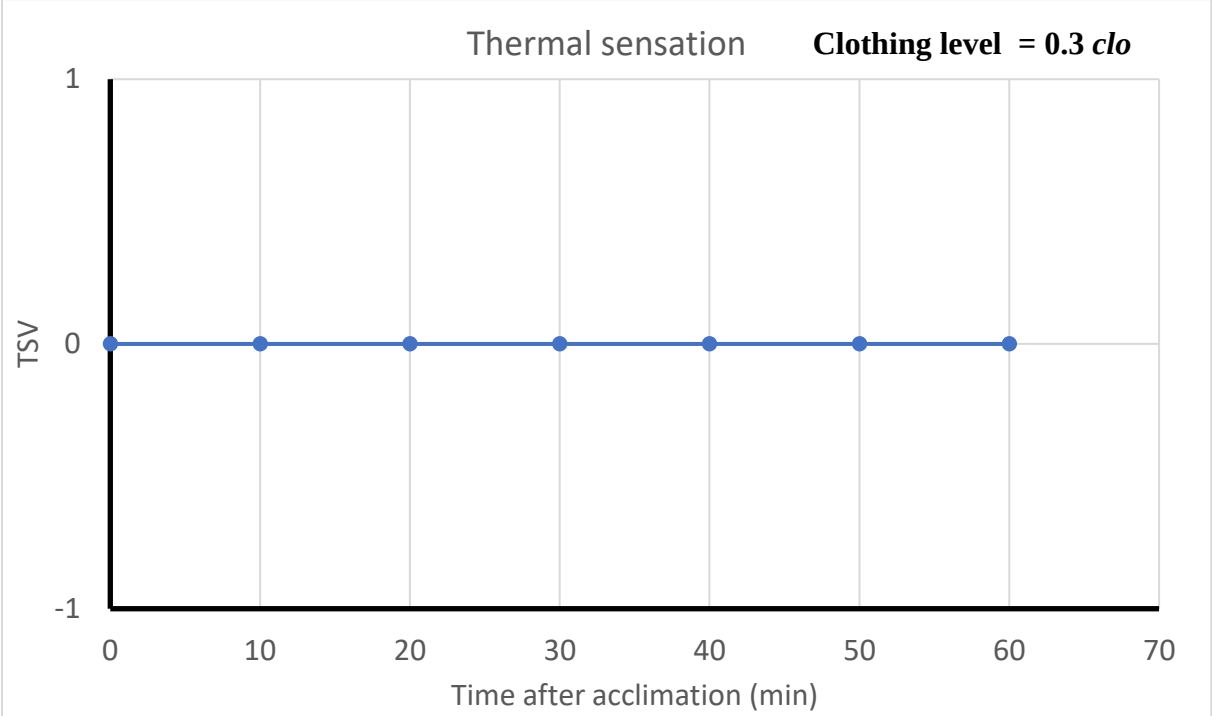

(d) TSV during the experiment

For the type 1 results, all subject's mean facial skin temperature did not have significant change but damped in the comfortable range determined by results in Chapter 3. The air temperature did not have much fluctuation during the whole experiment. Their thermal sensation votes were 0 during the whole experiment. Since their mean facial skin temperature did not have significant change, the setpoint temperature did not change during the experiment. This type of the results would be the most ideal one because the subject did not experience any discomfort.

Fig. 4.7 shows a typical response of the type 2 result. Fig. 4.7(a) shows the setpoint temperature, Fig. 4.7(b) shows the air temperature, Fig. 4.7(c) shows the mean facial skin temperature and Fig. 4.7(d) shows the TSV. The clothing level of this subject was 0.3 *clo* and the temperature setpoint calculated was 24.3 °C. The horizontal axis for all figures stands for the time passed after acclimation period in minutes and the vertical axis stands for temperature in Celsius for temperature results and stands for TSV for thermal sensation results.

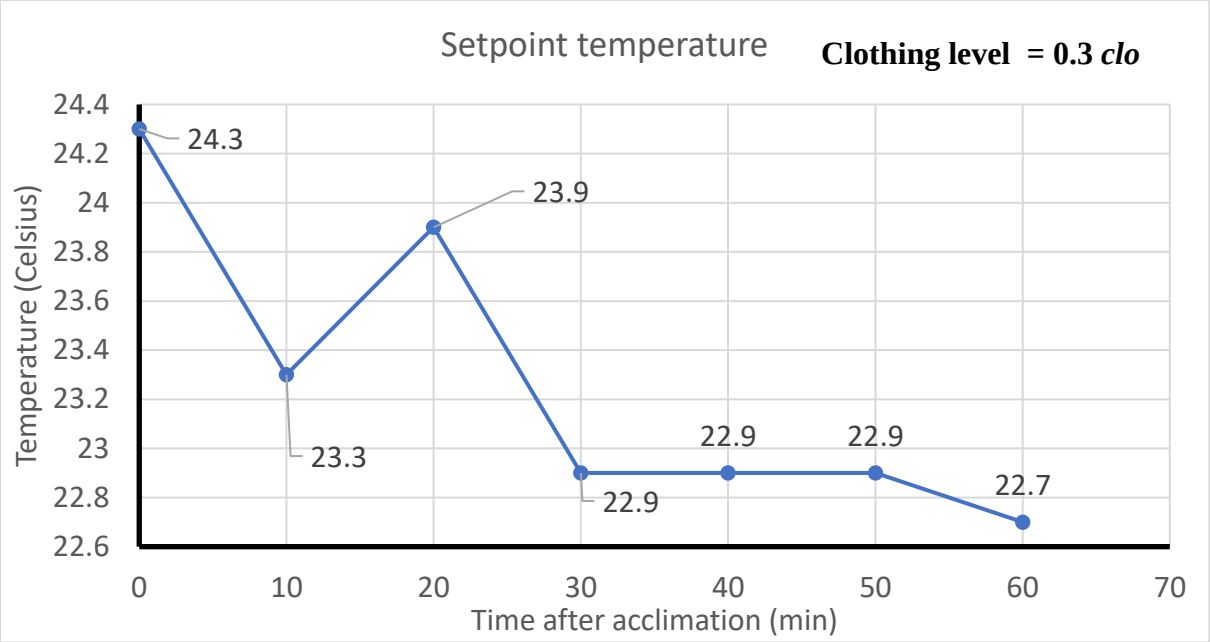

(a) Setpoint temperature

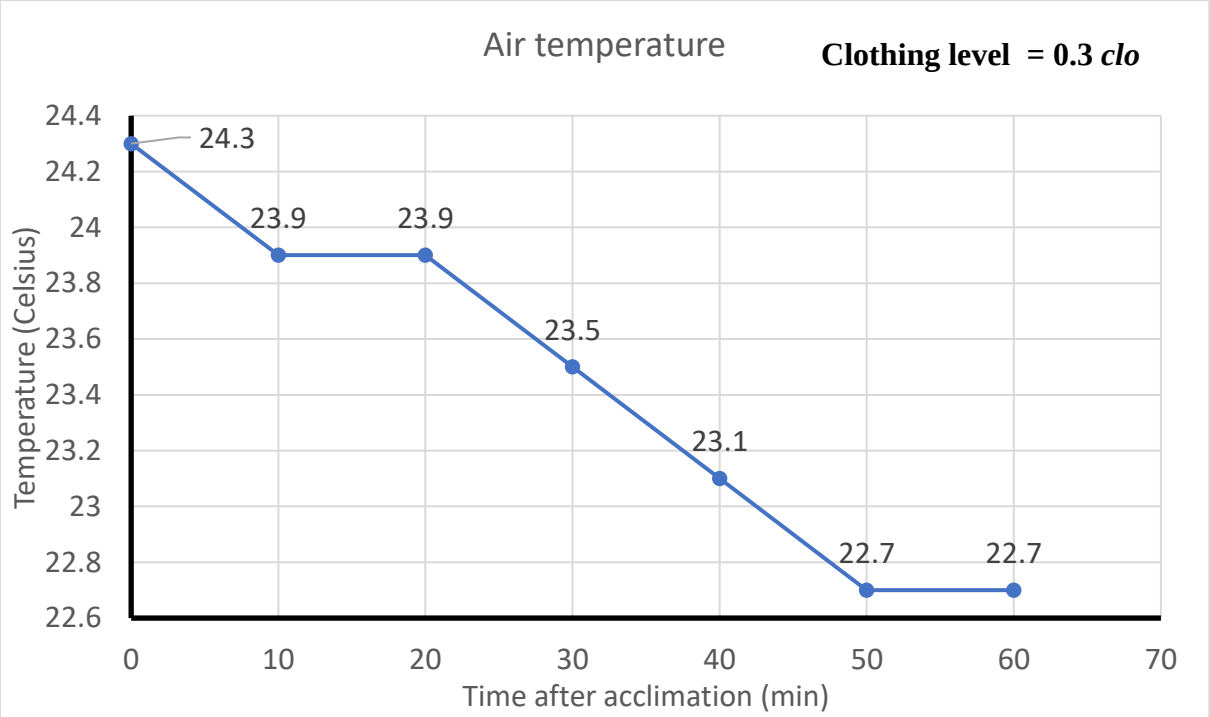

(b) Air temperature

Figure 4.7 Type 2 sample results

Figure 4.7 continued

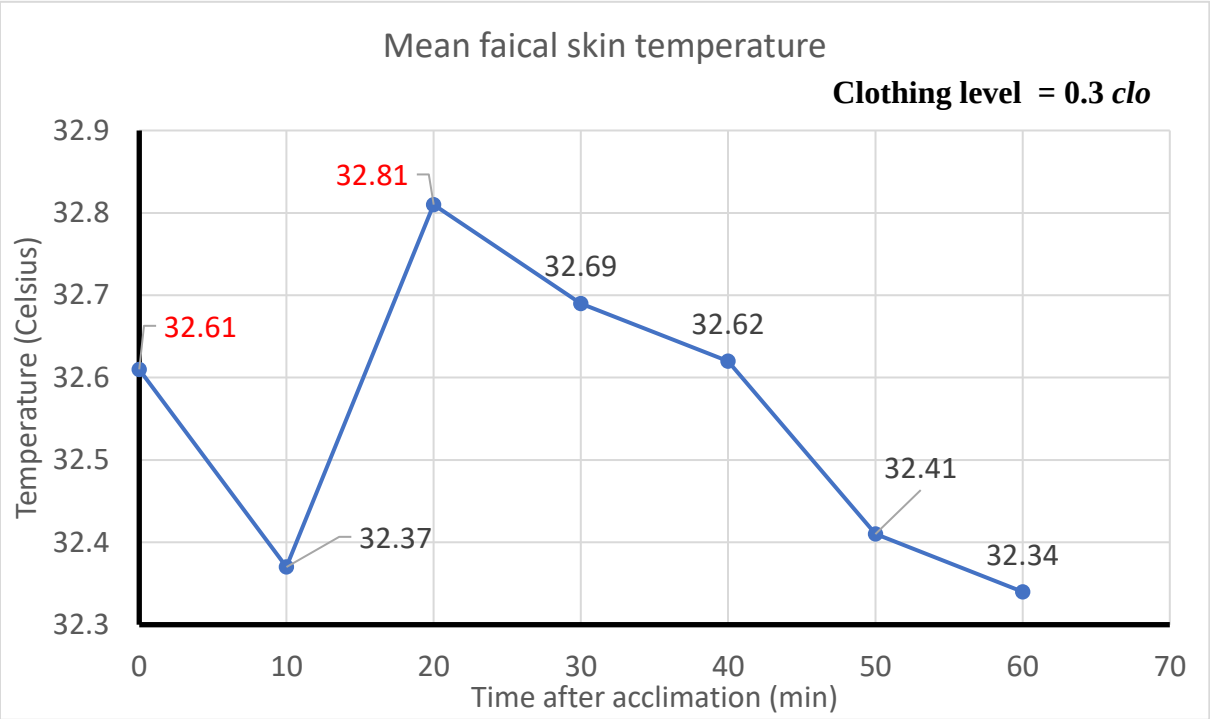

(c) Mean facial skin temperature

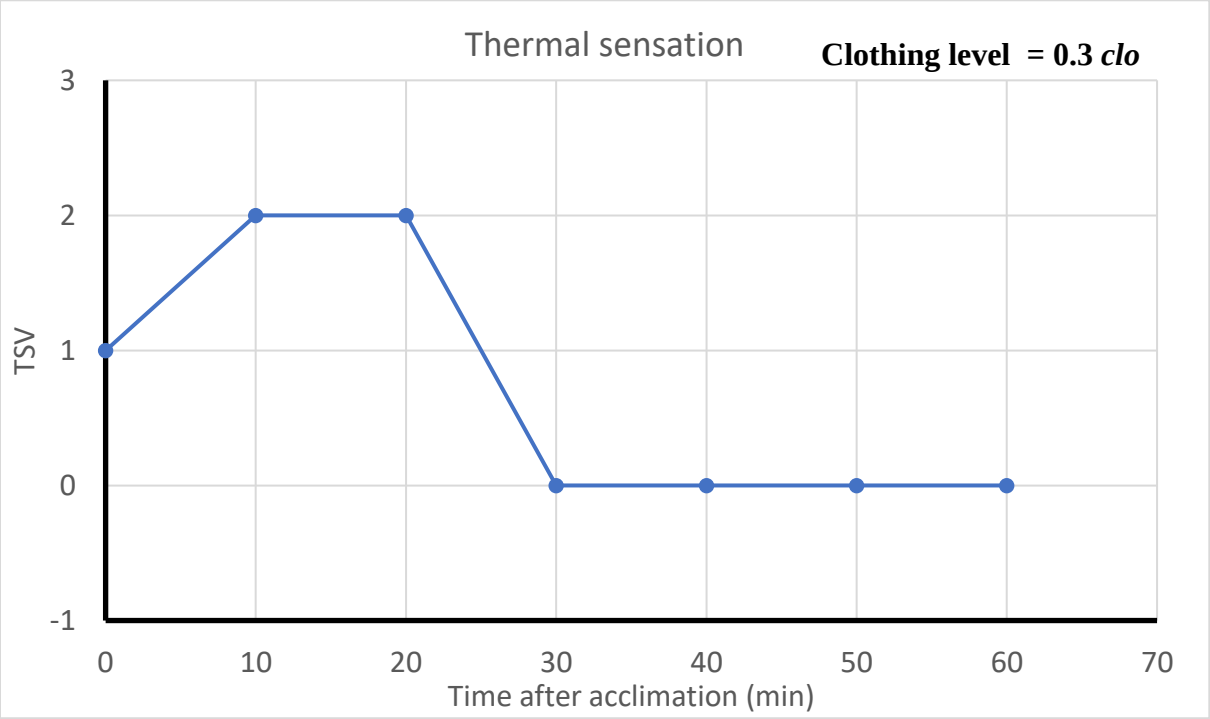

(d) TSV

At time 0, which was at the end of the acclimation period, the air temperature was controlled at 24.3, subject had a mean facial skin temperature reading at 32.61°C. Because this temperature was higher than comfortable threshold the setpoint decreased by 1°C. The subject also reported a TSV =1 which was slightly warm which met the prediction based on mean facial skin temperature. After 10 minutes, the subject reported a TSV = 2 which suggested the subject was feeling warm. However, the mean facial skin temperature was in the comfortable range, therefore the setpoint was adjusted to the air temperature at that time. At 20 minutes, the subjects mean facial skin temperature exceeded the threshold and the TSV was 2. Hence, the setpoint was decreased. At 30 and 40 minutes, occupant's mean facial skin temperature was still higher than the threshold. But because the air temperature did not reach the setpoint, the setpoint was not adjusted based on the improved logic. Occupant's TSV became 0, due to the cool air provided. At 50 minutes, occupant's mean facial skin temperature was in the comfortable range, thus the setpoint was adjusted to air temperature at that time. At the end, subject's TSV was 0. Type 2 results could consolidate the effectiveness of the control logic and the thermal comfort prediction based on mean facial skin temperature.

Fig. 4.8 shows a typical response of the type 3 result. Fig. 4.8(a) shows the setpoint temperature, Fig. 4.8(b) shows the air temperature, Fig. 4.8(c) shows the mean facial skin temperature and Fig. 4.8(d) shows the TSV. The clothing level of this subject was 0.4 *clo* and the temperature setpoint calculated was 23.8°C. The horizontal axis for all figures stands for the time passed after acclimation period in minutes and the vertical axis stands for temperature in Celsius for temperature results and stands for TSV for thermal sensation results.

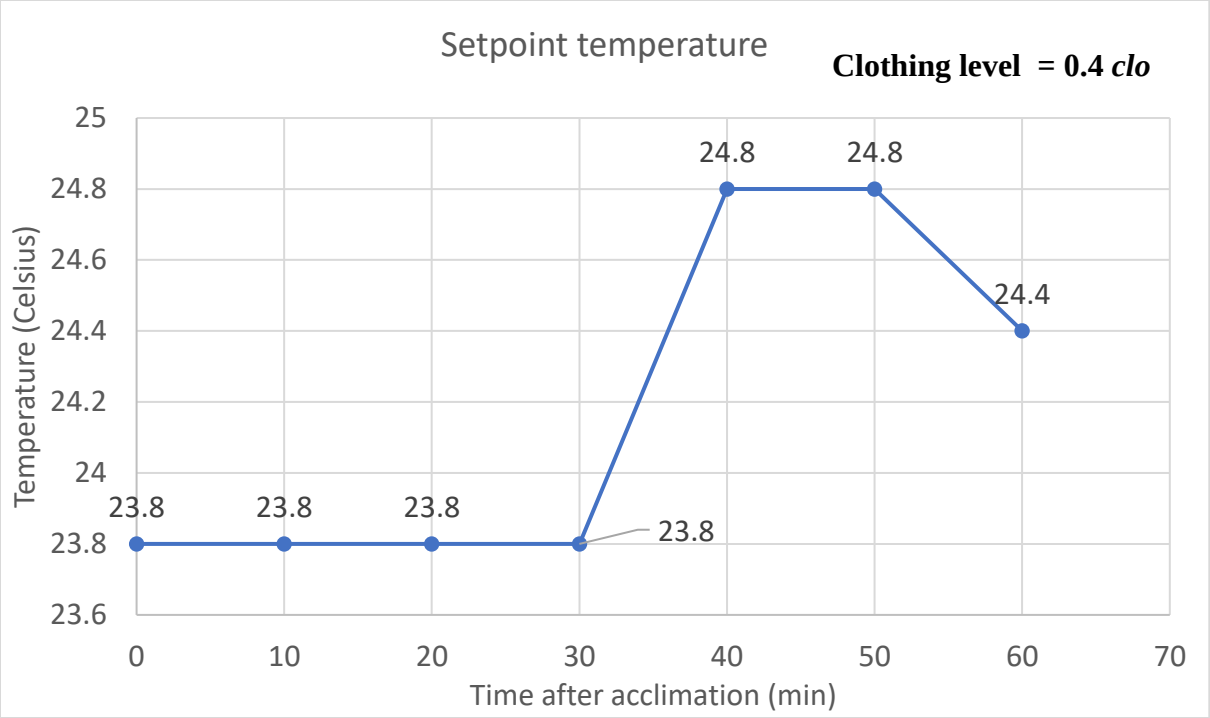

(a) Setpoint temperature

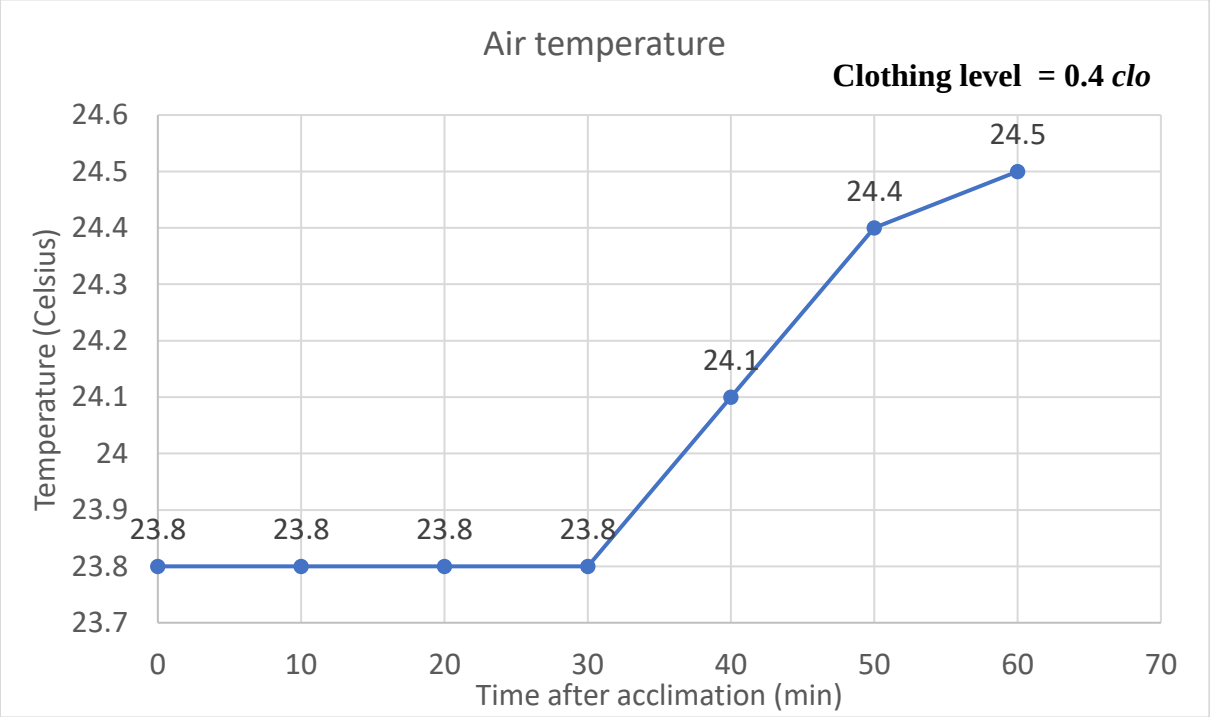

(b) Air temperature

Figure 4.8 Type 3 sample results

Figure 4.8 continued

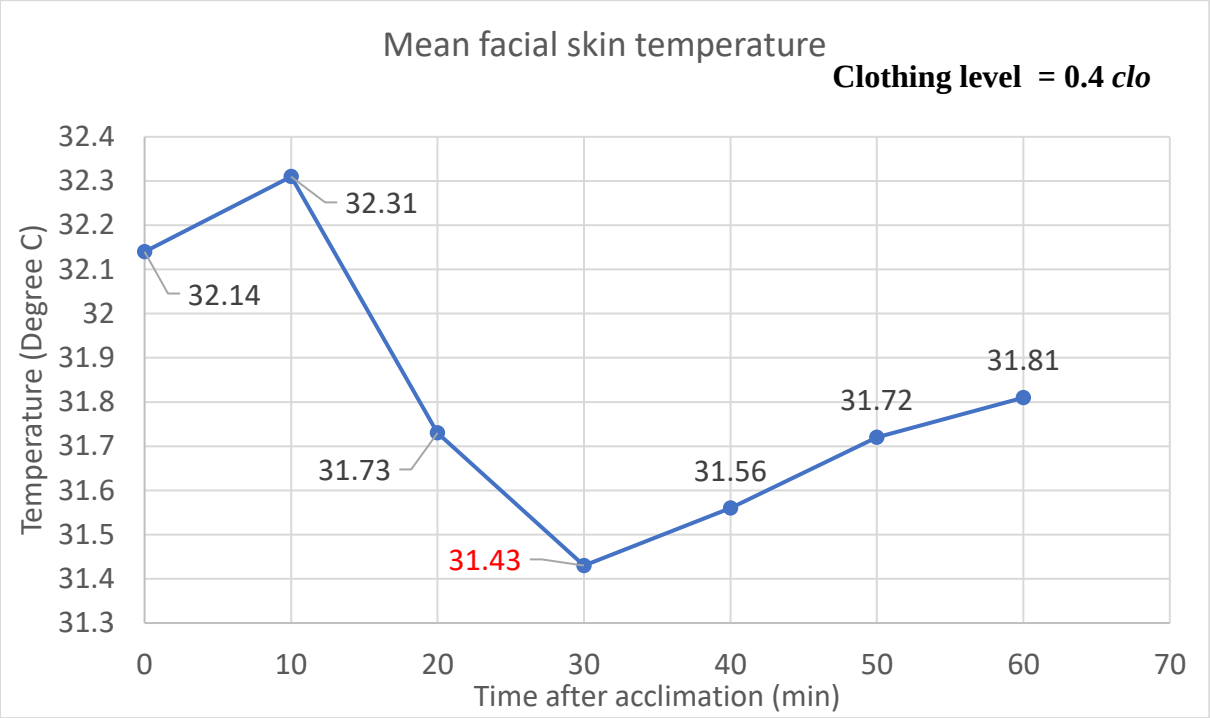

(c) Mean facial skin temperature

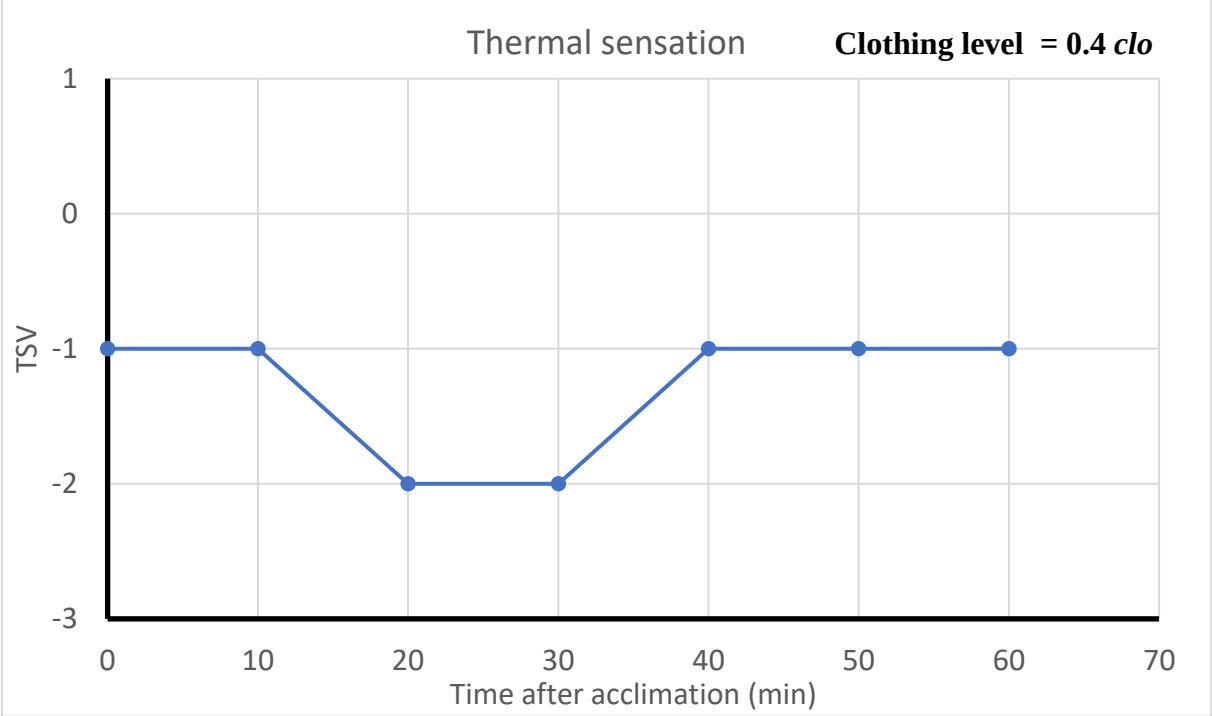

(d) TSV

During first 20 minutes, the air temperature was controlled at 23.8°C. However, the occupant reported TSV = -1 and -2. Based on this response, the setpoint temperature should be increased. Meanwhile, because the mean facial skin temperature was in the range, the control strategy did not adjust the setpoint temperature. At 30 minutes, the measured mean facial ski temperature was lower than the lower bond, therefore, the setpoint was increased. After the adjustment, even the subject's mean facial skin temperature raised back to the comfortable interval, the TSV was still not improved. At the end of the experiment, the occupant did not feel comfortable in this environment.

The tests show that 63.3% of subjects' TSVs were comfortable with the air temperature at setpoint that was determined by clothing level shown in Table 4.2. If a subject was not satisfied with the air temperature, the mean facial temperature of the subject could be used to adjust the setpoint according to Fig. 3.13. The adjustment could make an additional 27.3% of the subjects to feel comfortable. Thus, a total of 90.9% of the subjects could feel comfortable with the control strategy. The remaining 2 subjects reported uncomfortable with the control strategy so that the facial skin temperature was not a good indicator for their thermal comfort.

4.4 Discussions

This investigation performed experimental study to validate the proposed control strategy. Based on the results, there were two subjects who did not feel comfortable by using this strategy. This may be due to their personal preferences. Their skin temperatures seem in the comfortable range, but they still wanted cooler environments. Their thermal comfort requirement was a subjective feeling and may not be determined by physical parameters. Therefore, combing physiological parameters with other information such as occupant's location or air velocity could improve the control strategy.

Current HVAC systems also compromised the effectiveness of this strategy. Because the air temperature could not be adjusted fast enough. During the experiment, we noticed that it usually took one to two minutes before the systems started changing the air temperature. Even though it was a short period of time, the effect may still be huge. Overshooting the temperature was also a potential trouble, especially for heating cases. Because the test room used radiator to provide heat, it still emitted heat even after turned off. Such overshoot would cause fluctuation in the air

temperature and would make occupants uncomfortable. Thus, it would be ideal to have HVAC systems that has minimal overshoot.

Another issue was the location of LWIR camera. Because at current, the subject must look at the camera every 10 minutes to take measurement. Such interruption was not ideal for real environment. Also, if the subject was not facing the camera properly, the face detection could not find the face. In that case, it could not measure the temperature. Therefore, it might be helpful to have multiple cameras or cameras that could move to take pictures for the occupant.

Another consideration would be the privacy issue. Even though this strategy could provide a better environment, it used occupant's information to do so. Thus, it would be one of the worries when occupants used such system.

4.5 Conclusions

This chapter discussed about the implementation and the validation of the control strategy. The validation results proved the effectiveness of the control strategy with about 90.9% tested subjects felt comfortable by using this control strategy. From the experiment results, the correlation between the thermal comfort and the mean facial skin temperature was again confirmed. Also, the temperature setpoint determined based on the clothing level could be applied to most of the tested subjects. Furthermore, determining the clothing level by image classification program and measuring the mean facial skin temperature by LWIR camera combined with face detection program could be adopted in the HVAC control to provide a more comfortable environment.

CHAPTER 5. CONCLUSIONS AND FUTURE WORKS

This chapter summarizes the major conclusions in the research and provide some ideas for future works.

5.1 Conclusions

This study developed a new thermal environment control using occupant's mean facial skin temperature and clothing level. The control strategy automatically determined the comfortable temperature setpoint for different clothing level using image classification. This control strategy also adjusted the setpoint temperature automatically. The adjustment was based on the prediction of the thermal comfort.

This study trained a CNN image classification model using dataset classified by the clothing level. The results showed that the image classification model could determine the clothing level for the classes that the model was trained for. However, because the training dataset used in this study was small comparing to other large dataset, the trained model did not have comparable performance with another well-trained model. The training time was long but it could classify the image with acceptable speed. With this tool, this study performed experimental study of comfortable air temperature for different clothing level. The experimental study determined the relationship between clothing level and comfortable air temperature. The relationship was inverse which meant as the clothing level decreased, the comfortable air temperature increased. The relationship could be described using a second order parabolic trendline $y = 4.2185x^2 - 7.7836x + 26.239$. By using this curve, we could determine the air temperature that could provide a neutral sensation for specific clothing level. This study also compared the results with the PMV-PPD model. The results showed that the air temperature determined by this curve could produce an average PMV of -0.58 and an average PPD of 12.83% for six clothing levels. The discrepancy may due to the assumption that the mean radiant temperature and relative humidity was not considered during the experiment.

This study then investigated the relationship between mean facial skin temperature and thermal comfort. This study used LWIR camera to capture subject's facial temperature map. The LWIR

camera used in this study had a small size and good operability which made it very effective to perform experimental study. By using a Haar-cascade face detection model, the face location on the thermal map was determined. The model was effective and could produce results with fast speed. By using this tool, this study performed experimental study of mean facial skin temperature and thermal comfort, determined by TSV. The results showed that as the TSV increased from -2 to 2, the mean facial skin temperature increased from average 30.98°C to 33.25°C. For each TSV, the interval was not large but overlap existed between each thermal sensation. This overlap could be explained by personal preference of thermal comfort and personal difference on physiological differences. The results showed occupant was feeling neutral when mean facial skin temperature was between 31.7 and 32.5 °C. Therefore, measuring mean facial skin temperature using LWIR camera could non-invasively determine occupant's thermal comfort.

This study finally combined these two methods as well as the results to build a control platform using LabVIEW. This study developed a control logic specifically for this control strategy. This study them performed experimental study to validate the control strategy. The tests showed that 63.3% of subjects' TSVs were comfortable with the air temperature at the setpoint that was determined by clothing level. There were 27.3% of the subjects who were not satisfied with the air temperature, but the mean facial skin temperature of the subject was used to adjust the setpoint according to the results obtained from previous investigation. The adjustment made these 27.3% occupant felt comfortable again. Thus, a total of 90.9% of the subjects can feel comfortable with the control strategy. The remaining subjects did not feel comfortable by using this control strategy. This could also be explained by personal preferences that could not be determined based on physiological parameters.

5.2 Future Works

Although this study developed a new control strategy using mean facial skin temperature and clothing level and led to some conclusions. However, there are several aspects where the current work could be improved, or further research could be conducted.

First, the image classification model used in this study was a pretrained model. A pretrained model would not have performance as good as specifically designed model. Therefore, further researches on developing new structure or architecture of CNN to perform clothing level classification would

be possible. Also, there are other methods that could be used to determine clothing level, such as clothing temperature. Thus, it is also interesting to explore other approaches for better prediction of clothing level.

Second, this study only used mean facial skin temperature to determine thermal comfort. But it showed limitation on determining occupant's thermal preference and local discomfort. Therefore, to further improve the quality of thermal comfort, it is worth developing the methods to obtain such information and investigating the underlying relationship between these factors.

Third, this study only developed a control strategy for single occupant office. However, there are many offices with multiple occupants or open space offices. In those environments, the physiological parameters are hard to obtain. Also, for multiple occupants, the control logic needed to be reconsidered to optimize not only one occupant but multiple occupants. Furthermore, current control strategy only controlled air temperature, but because thermal comfort also relates to other factors, it is worth to developing a control method and strategy for other parameters to improve the thermal environment for multi-occupant offices.

LIST OF REFERENCES

Arens, E., Zhang, H., & Huizenga, C. (2006). Partial- and whole-body thermal sensation and comfort— Part I: Uniform environmental conditions. *Journal of Thermal Biology*, *31*(1-2), 53–59.

Arens, E., Humphreys, M. A., Dear, R. D., & Zhang, H. (2010). Are 'class A' temperature requirements realistic or desirable? *Building and Environment*, *45*(1), 4–10.

ASHRAE. (2013). *Standard 55 – Thermal environmental conditions for human occupancy.*

ASHRAE. (2009). F09 SI: Thermal Comfort. *ASHRAE handbook Fundamentals*, 9.1–9.30.

Azer, N. Z., & Hsu, S. (1977). The prediction of thermal sensation from a simple thermo-regulatory model. *ASHRAE Transactions*, *83*.

Bierman, W. (1936). The Temperature of the Skin Surface. *Journal of the American Medical Association*, *106*(14), 1158.

Brager, G., Zhang, H., & Arens, E. (2015). Evolving opportunities for providing thermal comfort. *Building Research & Information*, *43*(3), 274–287.

Carvalho, P. M. D., Silva, M. G. D., & Ramos, J. E. (2013). Influence of weather and indoor climate on clothing of occupants in naturally ventilated school buildings. *Building and Environment*, *59*, 38–46.

Cheng, Y., Niu, J., & Gao, N. (2012). Thermal comfort models: A review and numerical investigation. *Building and Environment*, *47*, 13–22.

Choi, J.-H., & Loftness, V. (2012). Investigation of human body skin temperatures as a bio-signal to indicate overall thermal sensations. *Building and Environment*, *58*, 258–269.

Chu, C.-M., & Jong, T.-L. (2008). Enthalpy estimation for thermal comfort and energy saving in air conditioning system. *Energy Conversion and Management*, *49*(6), 1620–1628.

Cosma, A. C., & Simha, R. (2018). Thermal comfort modeling in transient conditions using real-time local body temperature extraction with a thermographic camera. *Building and Environment*, *143*, 36–47.

Cosma, A. C., & Simha, R. (2019). Machine learning method for real-time non-invasive prediction of individual thermal preference in transient conditions. *Building and Environment*, *148*, 372–383.

Crow, F. C. (1984). Summed-area tables for texture mapping. *Proceedings of the 11th Annual Conference on Computer Graphics and Interactive Techniques - SIGGRAPH 84*.

Dear, R. D., & Brager, G. S. (2001). The adaptive model of thermal comfort and energy conservation in the built environment. *International Journal of Biometeorology*, *45*(2), 100–108.

Dear, R. D., Ring, J., & Fanger, P. (1993). Thermal Sensations Resulting from Sudden Ambient Temperature Changes. *Indoor Air*, *3*(3), 181–192.

Derrible, S., & Reeder, M. (2015). The cost of over-cooling commercial buildings in the United States. *Energy and Buildings*, *108*, 304–306.

Djongyang, N., Tchinda, R., & Njomo, D. (2010). Thermal comfort: A review paper. *Renewable and Sustainable Energy Reviews*, *14*, 2626–2640.

Enescu, D. (2017). A review of thermal comfort models and indicators for indoor environments. *Renewable and Sustainable Energy Reviews*, *79*, 1353–1379.

Fanger, P. O. (1982). *Thermal comfort: analysis and applications in environmental engineering*. Malabar, FL: Krieger.

Fanger, P. O., & Toftum, J. (2002). Extension of the PMV model to non-air-conditioned buildings in warm climates. *Energy and Buildings*, *34*(6), 533–536.

FLIR Systems. (2020). Lepton 3.5 LWIR camera. Retrieved from https://www.flir.com/

Gagge, A. P., Stolwijk, J. A. J., & Nishi, Y. (1971). An effective temperature scale based on a simple model of human physiological regulatory response. *ASHRAE Transactions*, *77*(1), 247–262.

GetLab. (2020). PureThermal 2 – FLIR Lepton Smart I/O Module. Retrieved from https://groupgets.com/manufacturers/getlab/products/purethermal-2-flir-lepton-smart-i-o-module

Givoni, B., & Goldman, R. F. (1971). Predicting metabolic energy cost. *Journal of Applied Physiology*, *30*(3), 429–433.

Guan, Y. Z., Hosni, M. H., Jones, B. W., & Gielda, T. P. (2003). Literature review of the advances in thermal comfort modeling. *ASHRAE Transactions*.

Hagino, M., & Hara, J. (1992). Development of a Method for Predicting Comfortable Airflow in the Passenger Compartment. *SAE Technical Paper Series*.

Harrison, G.A., Tanner, J.M., Pilbeam, D.R., & Baker, P.T. (1988) *Human Biology: An introduction to human evolution, variation, growth, and adaptability*. (3rd ed). Oxford: Oxford University Press

Harris, S. L., & Harris, D. M. (2018). *Digital design and computer architecture*. Amsterdam: Elsevier / Morgan Kaufmann Publishers.

Hoyt, T., Schiavon, S., Tartarini, F., Cheung, T., Steinfeld, K., Piccioli, A., & Moon, D. (2019). CBE Thermal Comfort Tool. Retrieved from https://comfort.cbe.berkeley.edu/

Huizenga, C., Hui, Z., & Arens, E. (2001). A model of human physiology and comfort for assessing complex thermal environments. *Building and Environment*, *36*(6), 691–699.

Indraganti, M., Ooka, R., Rijal, H. B., & Brager, G. S. (2014). Adaptive model of thermal comfort for offices in hot and humid climates of India. *Building and Environment*, *74*, 39–53.

ISO. (2005). Standard 7730. *Standard 7730 - Ergonomics of the thermal environment — Analytical determination and interpretation of thermal comfort using calculation of the PMV and PPD indices and local thermal comfort criteria*

Jazizadeh, F., & Jung, W. (2018). Personalized thermal comfort inference using RGB video images for distributed HVAC control. *Applied Energy*, *220*, 829–841.

Karjalainen, S. (2009). Thermal comfort and use of thermostats in Finnish homes and offices. *Building and Environment*, *44*(6), 1237–1245.

Katić, K., Li, R., & Zeiler, W. (2016). Thermo-physiological models and their applications: A review. *Building and Environment*, *106*, 286–300.

Kohri, I., & Mochida, T. (2002). Evaluation Method of Thermal Comfort in a Vehicle with a Dispersed Two-Node Model Part 1- Development of Dispersed Two-Node Model. *Journal of the Human-Environment System*, *6*(1), 19–29.

Kohri, I., & Mochida, T. (2003). Evaluation Method of Thermal Comfort in a Vehicle with a Dispersed Two-Node Model Part 2- Development of New Evaluation. *Journal of the Human-Environment System*, *6*(2), 77–91.

Klepeis, N. E., Nelson, W. C., Ott, W. R., Robinson, J. P., Tsang, A. M., Switzer, P., … Engelmann, W. H. (2001). The National Human Activity Pattern Survey (NHAPS): a resource for assessing exposure to environmental pollutants. *Journal of Exposure Science & Environmental Epidemiology*, *11*(3), 231–252.

Kontes, G., Giannakis, G., Horn, P., Steiger, S., & Rovas, D. (2017). Using Thermostats for Indoor Climate Control in Office Buildings: The Effect on Thermal Comfort. *Energies*, *10*(9), 1368.

Lecun, Y., Boser, B., Denker, J. S., Henderson, D., Howard, R. E., Hubbard, W., & Jackel, L. D. (1989). Backpropagation Applied to Handwritten Zip Code Recognition. *Neural Computation*, *1*(4), 541–551.

Lecun, Y., Bottou, L., Bengio, Y., & Haffner, P. (1998). Gradient-based learning applied to document recognition. *Proceedings of the IEEE*, *86*(11), 2278–2324.

Li, D., Menassa, C. C., & Kamat, V. R. (2018). Non-intrusive interpretation of human thermal comfort through analysis of facial infrared thermography. *Energy and Buildings*, *176*, 246–261.

Li, W., Zhang, J., & Zhao, T. (2019). Indoor thermal environment optimal control for thermal comfort and energy saving based on online monitoring of thermal sensation. *Energy and Buildings*, *197*, 57–67.

Li, Y., Li, F., Liu, Y., & Luo, Z. (2004). An integrated model for simulating interactive thermal processes in human–clothing system. *Journal of Thermal Biology*, *29*(7-8), 567–575.

Lin, M., Chen, Q., & Yan, S. (2013). Network in Network. *arXiv*, 1312.4400

Liu, W., Yang, D., Shen, X., & Yang, P. (2018). Indoor clothing insulation and thermal history: A clothing model based on logistic function and running mean outdoor temperature. *Building and Environment, 135,* 142–152.

Liu, S. (2018). Personal thermal comfort models based on physiological parameters measured by wearable sensors. *Proceedings of 10th Windsor Conference: Rethinking Comfort*.

Lomas, K. J., Fiala, D., & Stohrer, M. (2003). First principles modeling of thermal sensation responses in steady-state and transient conditions. *ASHRAE Transaction*, 79–187

McIntyre, D. A. (1978). Three approaches to thermal comfort. *ASHRAE Transactions, 84,* 101–109.

Ngarambe, J., Yun, G. Y., & Kim, G. (2019). Prediction of indoor clothing insulation levels: A deep learning approach. *Energy and Buildings*, *202,* 109402.

Nicol, J., & Humphreys, M. (2002). Adaptive thermal comfort and sustainable thermal standards for buildings. *Energy and Buildings*, *34*(6), 563–572.

Ogbonna A. C., & Harris D. J. (2008). Thermal comfort in sub-Saharan Africa: field study report in Jos–Nigeria. *Applied Energy*, *85,* 1–11.

Pasupathy, A., Velraj, R., & Seeniraj, R. (2008). Phase change material-based building architecture for thermal management in residential and commercial establishments. *Renewable and Sustainable Energy Reviews*, *12*(1), 39–64.

Peffer, T., Pritoni, M., Meier, A., Aragon, C., & Perry, D. (2011). How people use thermostats in homes: A review. *Building and Environment*, *46*(12), 2529–2541.

Peffer, T., Pritoni, M., Meier, A., Aragon, C., & Perry, D. (2011). How people use thermostats in homes: A review. *Building and Environment*, *46*(12), 2529–2541.

Putra, J. C. P. (2017). A Study of Thermal Comfort and Occupant Satisfaction in Office Room. *Procedia Engineering*, *170,* 240–247.

Ranzato, M., Huang, F. J., Boureau, Y.-L., & Lecun, Y. (2007). Unsupervised Learning of Invariant Feature Hierarchies with Applications to Object Recognition. *2007 IEEE Conference on Computer Vision and Pattern Recognition*.

Rawat, W., & Wang, Z. (2017). Deep Convolutional Neural Networks for Image Classification: A Comprehensive Review. *Neural Computation*, *29*(9), 2352–2449.

Salehi, B., Ghanbaran, A. H., & Maerefat, M. (2020). Intelligent models to predict the indoor thermal sensation and thermal demand in steady state based on occupants' skin temperature. *Building and Environment, 169,* 106579

Sandler, M., Howard, A., Zhu, M., Zhmoginov, A., & Chen, L.-C. (2018). MobileNetV2: Inverted Residuals and Linear Bottlenecks. *2018 IEEE/CVF Conference on Computer Vision and Pattern Recognition*.

Schiavon, S., & Lee, K. H. (2013). Dynamic predictive clothing insulation models based on outdoor air and indoor operative temperatures. *Building and Environment*, *59,* 250–260.

Schiavon, S., & Melikov, A. K. (2008). Energy saving and improved comfort by increased air movement. *Energy and Buildings*, *40*(10), 1954–1960.

Simard, P., Steinkraus, D., & Platt, J. (n.d.). Best practices for convolutional neural networks applied to visual document analysis. *Seventh International Conference on Document Analysis and Recognition, 2003. Proceedings.*

Simonyan, K., & Zisserman, A. (2014). Very deep convolutional networks for large-scale image recognition. *arXiv*, 14409.1556

Smith, C. E. (1991). A transient, three-dimensional model of human thermal system. PH.D. Dissertation, Kansas State University, Manhattan, Kansas.

Smith, L.N. (2018). A disciplined approach to neural network hyper-parameters: Part 1 -- learning rate, batch size, momentum, and weight decay. *arXiv*, 1803.09820

Srivastava, N., Hinton, G., Krizhevsky, A., Sutskever, I., & Salakhutdinov, R. (2014). Dropout: A simple way to prevent neural networks from overfitting. *Journal of Machine Learning Research*, *15*(1), 1929–1958.

Stolwijk, J. A. J. (1971). A mathematical model of physiological temperature regulation in man, NASA Contractor Report, NASA CR-1855. *Washington, DC: National Aeronautics and Space Administration.*

Taniguchi, Y., Aoki, H., Fujikake, K., Tanaka, H., & Kitada, M. (1992). Study on Car Air Conditioning System Controlled by Car Occupants Skin Temperatures - Part 1: Research on a Method of Quantitative Evaluation of Car Occupants Thermal Sensations by Skin Temperatures. *SAE Technical Paper Series*.

Viola, P., & Jones, M. (n.d.). Rapid object detection using a boosted cascade of simple features. *Proceedings of the 2001 IEEE Computer Society Conference on Computer Vision and Pattern Recognition. CVPR 2001*.

Wang, F., Zhu, B., Li, R., Han, D., Sun, Z., Moon, S., … Yu, W. (2017). Smart control of indoor thermal environment based on online learned thermal comfort model using infrared thermal imaging. *2017 13th IEEE Conference on Automation Science and Engineering (CASE)*.

Wang, X. L., & Peterson, F. K. (1992). Estimating thermal transient comfort. *ASHRAE Transactions, 98*(1), 7.

Wang, X. L. (1994). Thermal comfort and sensation under transient conditions. Ph.D. dissertation, Department of energy technology, division of heating and ventilation, The Royal Institute of Technology, Sweden

Walikewitz, N., Jänicke, B., Langner, M., Meier, F., & Endlicher, W. (2015). The difference between the mean radiant temperature and the air temperature within indoor environments: A case study during summer conditions. *Building and Environment*, *84*, 151–161.

Wyon N. M., and Wyon D. P., 1987, "Measurement of acute response to draught in the eye", *Acta Ophthalmologica, 65*(4), 385–392

Xiong, J., Lian, Z., Zhou, X., You, J., & Lin, Y. (2016). Potential indicators for the effect of temperature steps on human health and thermal comfort. *Energy and Buildings*, *113*, 87–98.

Xu, W., Chen, X. & Zhao, J. (2010). An adaptive Predicted Mean Vote (aPMV) model in office. *2010 International Conference on Mechanic Automation and Control Engineering*.

Yao, R., Li, B., & Liu, J. (2009). A theoretical adaptive model of thermal comfort – Adaptive Predicted Mean Vote (aPMV). *Building and Environment*, *44*(10), 2089–2096.

Yao, Y., Lian, Z., Liu, W., & Shen, Q. (2008). Experimental study on physiological responses and thermal comfort under various ambient temperatures. *Physiology & Behavior*, *93*(1-2), 310–321.

Yi, B., & Choi, J.-H. (2015). Facial Skin Temperature as a Proactive Variable in a Building Thermal Comfort Control System. *Sustainable Human–Building Ecosystems*, 117–125.

LIST OF PUBLICATIONS

Li, X., Deng, Z., Shi, Z., & Chen, Q. (2019). Advanced indoor thermal environment control using occupant's mean facial skin temperature and clothing level. Abstract accepted by *Indoor Air 2020 (Korea, 2020)*.